

Long-range transport of dust aerosols over the Arabian Sea and Indian region - A case study using satellite data and ground-based measurements

K.V.S. Badarinath¹, Shailesh Kumar Kharol¹, D.G. Kaskaoutis², Anu Rani Sharma¹, V. Ramaswamy³ and H.D. Kambezidis²

¹Atmospheric Science Section, Oceanography Division,
National Remote Sensing Centre (Dept. of Space-Govt. of India) Balanagar, Hyderabad –
500 037, India. Email: badrinath_kvs@nrsa.gov.in

²Atmospheric Research Team,
Institute for Environmental Research and Sustainable Development,
National Observatory of Athens,
Lofos Nymphon, P.O. Box 20048, GR-11810 Athens, Greece

³National Institute of Oceanography, Goa, India

Abstract

The present study addresses an intense dust storm event over the Persian Gulf and the Arabian Sea (AS) region and its transport over the Indian subcontinent using multi-satellite observations and ground-based measurements at a central urban location, Hyderabad, India. A time series of Indian geostationary satellite KALPANA-1 Very High Resolution Radiometer (VHRR) together with ground observations are used to analyze the temporal variation of the dust event that occurred from 19 to 24 February 2008 with the strongest intensity on 22 February. The Ozone Monitoring Instrument (OMI) Aerosol Index (AI) is also examined to provide an independent assessment of dust presence and plume location. During the dust event drastic increase in Terra/Aqua-MODIS AOD₅₅₀ and AURA-OMI AI were observed. Vertically-resolved attenuated backscatter during daytime and nighttime from Cloud-Aerosol Lidar and Infrared Pathfinder Satellite Observation (CALIPSO) data are also used as an additional tool to monitor the dust vertical distribution over the Indian region. The main dust layer was observed to be situated between 3–5 km in altitude with traces of dust particles reaching 6–7 km. The CALIPSO observations on vertical profile of aerosols are in qualitative agreement with values of MODIS-AOD₅₅₀ and OMI-AI. Ground-based measurements showed significant reduction in solar irradiance on the dust-laden day (22 February 2008) over Hyderabad. Sun photometer derived AODs from six AERONET sites in south Asia verified the presence of dust and its transport from west to east. The predictions of the Dust Regional Atmospheric Model (DREAM) model are consistent with the satellite observations, thus implying the appropriateness of the model to monitor the dust transport over the region.

Keywords: Dust event; KALPANA-1 VHRR; MODIS; AURA-OMI; CALIPSO; Arabian Sea; India

1. Introduction

Despite the increased anthropogenic emissions due to the growth of population the air quality is also affected by mineral particles from dust storms and smoke from naturally occurring biomass burning (Ichoku et al., 2004). Satellite-based measurements for monitoring these atmospheric constituents are a viable proposition since ground-based measurements are limited in space and time (Liu et al., 2008; Papadimas et al., 2008). Deserts in western Asia produce large amounts of mineral dust particles that enter the atmosphere. Dust is considered to be one of the major sources of tropospheric aerosol loading, and constitutes an important key parameter in climate aerosol-forcing studies (Kaufman et al., 2002; Tegen, 2003; Huang et al., 2006; Slingo et al., 2006). However, there is still a large-scale uncertainty in the estimation of radiative forcing caused by dust particles mainly due to their non-sphericity and the different chemical composition (Washington et al., 2003).

The impact of mineral dust aerosols in the Earth's system depends mainly on particle characteristics such as size, shape and mineralogy (Mahowald et al., 2005), which are initially determined by the terrestrial sources from which the soil sediments are entrained. Whilst these characteristics can change during dust transport (Mackie et al., 2008) they are initially determined by their source regions. Therefore, due to the high spatial variability of the dust plume characteristics along its transport, remote sensing is an established method for the detection and mapping of dust events (Moulin et al., 1998; Badarinath et al., 2007a; Kaskaoutis et al., 2008) and has recently been used to identify the dust-source locations with a varying degree of success (Washington et al., 2003; Alpert et al., 2004; Bullard et al., 2008; Baddock et al., 2008). To this respect, the passage of dust over land and ocean and the variation along its transport have been monitored by satellite sensors with resolutions varying from low to high; amongst others AVHRR (Evan et al., 2006), COES-VISSR (McKinnon et al., 1996), METEOSAT (Moorthy et al., 2007), MODIS (Kaskaoutis et al., 2008), MSG-SEVIRI (Schepanski et al., 2007), SeaWiFS (Antoine and Nobileau, 2006). However, the ability of the satellite data to detect dust plume is limited by several factors, such as the radiative properties of the dust and the underlying land/ocean surface, the cloud presence, the density of the dust plumes and the algorithms used in the aerosol retrievals. Therefore, dust monitoring is better achieved by the combined use of remote sensing and surface meteorological data, such as wind speed and visibility (Mahowald et al., 2007), AERONET measurements (Kim et al., 2007) and lidar systems (Pérez et al., 2006).

Desert dust can be transported by the mean wind to thousands of kilometers away from the source regions. This transport plays an important role in the regional and global radiative balance both at the top of the atmosphere (TOA) and at the surface (Mattis et al., 2002). Dust aerosols strongly affect visibility, perturb the radiation balance in the Earth-Atmosphere system, and also cause serious biological and ecological effects (Badarinath et al., 2007a). Desert dust can affect soil nutrients at source and sink regions (Muhs et al., 2007) and may regulate the phytoplankton activity in the oceans (Donaghay et al., 1991). For example, mineral dust from the Sahara has shown to contribute significantly to the nutrient budget of equatorial forests in Africa and Amazonia (Harrison et al., 2001; Piketh and Walton, 2004). The desert-dust aerosols have also been associated with an increase in coral mortality and *Trichodesmium* blooming in the Caribbean (Lenes et al., 2001; Griffin et al., 2003; Shinn et al., 2000). Soil dust transported at thousands of kilometers away from the source region can also convey pathogens and pollen from genetically-modified crops. Perhaps, the most interesting aspect is the study of dust as a source of iron to high-nutrient, low-chlorophyll (HNLC) oceans, where plankton productivity is limited because of the availability of soluble iron (Lenes et al., 2001). Furthermore, dust particles affect cloud microphysical properties (Levin and Ganor, 1996), atmospheric heating and stability (Alpert et al., 2004), tropical cyclone activity (Badarinath et al., 2008), air quality (Astitha et al., 2008), photolysis rates, ozone chemistry and human health (Rodriguez et al., 2001). The significant dust effects on global climate, meteorology and atmospheric dynamics, ecosystems and human health are highlighted in detail in review studies (Goudie and Middleton, 2001; Engelstaedter et al., 2006).

A dust storm is a meteorological phenomenon considered as natural hazard, which can affect everyday life for a short-time interval ranging from a few hours to a few days. Dust and sand storms are a persistent problem in Iraq and other areas in the Middle East and are most prevalent in the spring and summer months due to the strong northwesterly winds known as “shamal winds” (NOAA Report, 86). The shamal winds are caused by a wave of high pressure that funnels through the Persian Gulf between Saudi Arabia and Iran, and are the most hazardous weather conditions in the region. This seasonal trend can best be characterized as a combination of two separate weather systems: the sub-tropical jet stream pushing up south of the Arabian Peninsula and a polar front jet stream pushing southward from the European continent causing the strong shamal winds. Though not much is reported about the interannual or decadal variability of dust episodes, preliminary indications suggest that dust episodes are increasing in frequency and magnitude, especially in the countries bordering the northern Arabian Sea. These regions are characterized by numerous river-fed endorheic basins. Due to construction of dams and

diversion of water for agriculture, the lakes have significantly decreased in size and the dried-up lake beds are now major sources of eolian dust in south Asia; similar phenomena have been observed in Australia with the lake Eyre (Baddock et al., 2008) and in Chad “chotts” (Engelstaedter et al., 2006; Prospero et al., 2002). Therefore, it is obvious that the aerosol studies over south Asia and India provide a great scientific importance due to the combined effects of aerosols of different origin, i.e. anthropogenic activities and fossil-fuel combustions due to the great growth of population and industrialization, marine aerosols from the neighboring seas (Bay of Bengal, Indian Ocean, Arabian Sea), biomass-burning aerosols from the seasonal forest fires, and desert particles from the northwestern arid regions. Despite that several in-situ and on-board studies as well as experimental campaigns have investigated aerosols, mainly biomass burning and sea salt (Satheesh et al., 2006a; Badarinath et al., 2007b among others) and air pollution, mainly Black Carbon, mass concentration and PM₁₀, (Latha and Badarinath, 2005a; Badarinath et al., 2007b, c; Kharol and Badarinath, 2006, 2007) in continental India and adjoining oceanic regions, only few have focused on examining the dust transport (El-Askary et al., 2006; Prasad et al., 2007). Between them we can highlight a recently published work regarding the dust transport from the Thar Desert on 9-11 April 2006 over Hyderabad (Badarinath et al., 2007a).

In the present study, data from the Indian geostationary satellite KALPANA-1 VHRR are used to analyze the spread of mineral-dust particles over the Persian Gulf, AS and northwestern part of India from a strong dust outbreak occurred during the period between 19-24 February 2008. CALIPSO observations are also analyzed in order to provide the vertical profile of aerosols over the region. Furthermore, satellite data from MODIS and OMI sensors are used to understand the spatial distribution of aerosols during the dust event. The Mesoscale Model 5 (MM5) is also used in order to provide the synoptic meteorological systems that have controlled the long-range transport of dust. Solar radiation measurements were performed over Hyderabad to examine the variations caused by the dust presence. The west-to-east dust-plume transport that occurred in the south Asia region was monitored via sun photometric measurements at six AERONET stations over the region. The Dust REgional Atmospheric Model (DREAM) is finally used to verify the presence as well as the variation of the dust event in the south Asia region.

2. Datasets and methodology

2.1. Satellite-based measurements

Mineral and desert dust can be detected via satellite observations in the ultraviolet (0.315- 0.4 μm) via absorption, visible (0.38-0.79 μm) via scattering and thermal infrared via contrasting land/aerosol emissivity (Baddock et al., 2008). In order to evaluate, compare and contrast the mineral aerosols for the dust event in south Asia, several remote-sensing data described in the following sections are used in the present study.

2.1.1. MODIS

MODIS has been acquiring nearly daily or global coverage data in 36 spectral bands from visible to thermal infrared (29 spectral bands with 1-km, 5 spectral bands with 500-m, and 2 spectral bands with 250-m, nadir pixel dimensions). The MODIS sensor is onboard the polar orbiting NASA-EOS Terra and Aqua spacecrafts with equator crossing times of 10:30 and 13:30 Local Solar Time, respectively (Levy et al., 2007). A nearly global image is produced due to the larger swath widths of MODIS and instrument-scanning angle of 110° (Levy et al., 2003). The MODIS images have extensively been used for monitoring of forest fires, dust outbreaks, severe storms, cyclones, volcanoes etc (Badarinath et al., 2007a, 2008; Kaskaoutis et al., 2008). Aerosol retrievals from MODIS data are performed over land and ocean surfaces by means of two separate algorithms described in literature (Kaufman and Tanré, 1998). The aerosol properties are derived by the inversion of the MODIS-observed reflectance using pre-computed radiative transfer look-up tables based on aerosol models (Remer et al., 2005; Levy et al., 2007). The initial versions of the MODIS algorithms have been under continued development, and have recently received an improved aerosol determination, via processing to Collection 5 (C005) (Levy et al., 2007). The data used in this study include both Terra and Aqua MODIS aerosol products, calculated using separate algorithms over land and ocean to obtain AOD at 550 nm (AOD₅₅₀) and the proportion of AOD₅₅₀ contributed to the fine-mode aerosols (determined as fine-mode fraction, FM); such estimations are only made over cloud-free regions (Remer et al., 2005). The C005 Level 3 (spatial resolution 1°x1°) MODIS products are obtained from Giovanni website (<http://giovanni.gsfc.nasa.gov/>) during the dust event over south Asia.

2.1.2. OMI

In addition to MODIS data, UV Aerosol Index (AI) values from the Ozone Monitoring Instrument (OMI) onboard the Finnish-Dutch AURA satellite are used. The AURA satellite, launched in July 2004, flies a few minutes behind the Aqua satellite as part of the NASA A-Train constellation. OMI was designed to replace the Total Ozone Mapping Spectrometer (TOMS) to continue recording total ozone and other atmospheric parameters related to ozone chemistry and climate. Furthermore, and unlike MODIS, OMI-AI is sensitive to aerosol absorption even when the particles are above cloud; thus AI can be derived successfully in both cloudless and cloudy conditions (Torres et al., 2007). OMI has a spatial resolution of 13 x 24 km at nadir and uses the same retrieval algorithm with TOMS (Torres et al., 1998). OMI measures back scattered radiances in the near UV region, and using these measurements, the retrieval algorithm computes an absorbing AI, which is a qualitative measure of the presence of UV-absorbing aerosols, such as mineral dust and smoke over all terrestrial surfaces, including deserts and snow- ice covered areas. The absorbing AI from the current OMI sensor is defined as the difference between measured (includes aerosol effects) spectral contrast at 360- and 331- nm radiances and the contrast calculated from the radiative transfer theory for a pure molecular (Rayleigh) atmosphere (Ahmad et al., 2003). AI is calculated using the ratio of upwelling radiances at 331 and 360 nm as:

$$AI = -100[\log_{10}(I_{360}/I_{331})_{meas} - \log_{10}(I_{360}/I_{331})_{calc}] \quad (1)$$

Since the calculation of I_{360} uses the reflectivity derived from the I_{331} measurements, the AI definition essentially simplifies to:

$$AI = 100 \log_{10}(I_{360_meas}/I_{360_calc}) \quad (2)$$

Where, the subscripts ‘meas’ and ‘calc’ refer to measured and calculated values of the upwelling radiances, respectively.

AI detects UV-absorbing aerosols thus providing an independent information relating to mineral-dust detection. The AI is positive for absorbing aerosols and negative for non- absorbing, while values of AI near zero indicate cloud presence. In interpreting these results, care has to be taken at some surface effects, such as sea glint and ocean color, which can enhance AI. The present study uses the OMI-AI Level 3 global-gridded product (0.25° x 0.25° spatial resolution). In general, OMI-AI and MODIS-AOD

data are somewhat complementary; the first are ideal for initial dust detection and the second can be used to both identify plumes and sources at higher spatial resolution.

AI is sensitive to a range of UV-absorbing aerosols such as mineral dust, volcanic ash, and black carbon from fossil-fuel combustion sources and biomass burning (Eck et al., 2001). The UV surface reflectivity is typically low and nearly constant over both land and sea, which allows OMI to detect aerosols over both land and ocean (Torres et al., 2007). The main utility of the AI is the detection of dust, especially in an elevated atmospheric layer. Average AI values over long-time periods have been used to detect persistent dust sources (Washington et al., 2003; Alpert et al., 2004; Baddock et al., 2008). Extensive analysis of the seasonal and interannual variability of TOMS-AI values has been made over India by Habib et al. (2006). The present study evaluates the quality of the OMI-AI to detect the dust-source regions and, furthermore, examines its application to mid- and large-scale aerosol transport in south Asia.

2.1.3. KALPANA-1

KALPANA-1 (formerly METSAT-1), an exclusive Indian meteorological satellite was launched by PSLV, on 12 September 2002. The satellite comprises one Very High Resolution Radiometer (VHRR) and a Data Relay Transponder (DRT) payload to meet meteorological requirements. VHRR operates in three bands, (a) the visible (0.55 – 0.75 μm), (b) the thermal infrared (10.5 – 12.5 μm) and (c) the water-vapor infrared bands (5.70 - 7.10 μm), with a spatial resolution of 2 x 2 km for the visible band and 8 x 8 km for the thermal infrared and water-vapor ones, to obtain atmospheric cloud cover, water vapor and temperature (Bhattacharya et al., 2008). The DRT also provides data from fixed/mobile ground-level weather platforms.

2.1.4. CALIPSO

The Cloud-Aerosol Lidar and Infrared Pathfinder Satellite Observation (CALIPSO) provide new insight of the role of clouds and atmospheric aerosols (airborne particles) in regulating Earth's weather, climate, and air quality. As part of the A-train satellite constellation that includes the Aqua, CloudSat, Aura, Orbiting Carbon Observatory (OCO) and PARASOL satellites, CALIPSO has a 98°-inclination orbit and flies at an altitude of 705 km providing the vertical distribution of aerosols and clouds. CALIPSO was launched on 28 April, 2006. The CALIPSO payload consists of three instruments: the Cloud-

Aerosol Lidar with Orthogonal Polarization (CALIOP), an Imaging Infrared Radiometer (IIR), and a moderate spatial resolution Wide Field-of-view Camera (WFC). CALIOP provides profiles of backscatter at 532 and 1064 nm, as well as two orthogonal (parallel and perpendicular) polarization components at 532 nm. A detailed discussion of CALIOP data products has been described elsewhere (Vaughan et al, 2004).

2.2. Ground-based measurements

2.2.1. MICROTOPS-II

Synchronous and continuous observations of AOD are carried out in Hyderabad, India, using a handheld multichannel Solar Light microprocessor-controlled total ozone portable spectrometer (MICROTOPS-II) at six wavelength bands centered on 380, 440, 500, 675, 870 and 1020nm. The sun photometer works on the principle of measuring surface-reaching solar radiation intensity at specified wavelength bands and calculates corresponding optical depths by knowing the respective radiation intensities at TOA. The TOA irradiances at each wavelength are calculated via the well-known Langley method (Reagan et al., 1986; Russell et al., 1993; Schmid and Wehrli, 1995). As per the details provided by the supplier, the calibration relies on a high-performance voltage reference with the temperature coefficient $>0.001\%$ per degree Celsius and long-term stability of $\sim 0.005\%$ per year. The Full Width at Half Maximum (FWHM) bandwidth at each of these wavelength channels is 2.4 ± 0.4 nm, and the accuracy of the sun-targeting angle is better than 0.1° . Great care has also been taken to avoid any error in sun, targeting the MICROTOPS-II by mounting the instrument on a tripod stand. Details concerning the design, calibration, and performance of MICROTOPS-II have been described elsewhere (Morys et al., 2001). A detailed analysis for the calculation of the spectral AOD using the MICROTOPS-II is given in Badarinath et al. (2007b).

2.2.2. MFRSR

Multi-Filter Rotating Shadow band Radiometer (MFRSR) measurements at wavelengths of 415.9, 496.6, 622.4, 670.2, 868.3, and 938.5 nm (FWHM ~ 10 nm) are used for measurements of total, diffuse horizontal, and direct-beam solar irradiances (Harrison et al., 1994) in Hyderabad, India. The instrument's sensors are shaded at periodic intervals by a rotating shadow band so the diffuse incoming radiation is measured. The principal sources of uncertainty in the MFRSR detector are the cosine-

response error, the instrument-leveling error and an error associated with blocking part of the sky when shading the sun. Yankee Environmental Systems, Inc. provides the measured (to zenith) cosine response for each MFRSR channel and these values are used to estimate the error in diffuse fraction (diffuse-to-global irradiance) that results from this nonideal cosine response. The direct radiation component, which is computed as the difference between the sun blocked (shaded) and unshaded radiometer is corrected for the cosine-response error, but the diffuse component is not. The MFRSR has already been used in several publications in Hyderabad (e.g., Badarinath et al., 2007a, b).

2.2.3. CIMEL

The AERONET measurements reported in this work are made with the CIMEL sun photometer (CE-318), which is an automatic sun-sky scanning spectral radiometer. The CIMEL sun photometer takes measurements of the direct-sun and diffuse-sky radiances every 15 minutes within the spectral range 340-1020 nm and 440-1020 nm, respectively. The direct-sun measurements are performed in eight spectral channels: 340, 380, 440, 500, 675, 870, 940 and 1020 nm. Seven of the eight bands are used to acquire AOD, while that at 940 nm is used to estimate the total precipitable water content. The Ångström parameter is computed from AODs at 440 and 870 nm. The filters utilized in these instruments are ion-assisted deposition-interference filters with a FWHM of 10 nm except for the 340-nm and 380-nm filters having a FWHM of 2 and 4 nm, respectively. The instrumentation, data acquisition, retrieval algorithms and calibration procedure conform with the standards of the AERONET and are described in detail in numerous studies (e.g., Dubovik et al., 2000; Holben et al., 2001). Typically, the total uncertainty in AOD for a field instrument under cloud-free conditions is ± 0.01 for $\lambda > 440$ nm, and ± 0.02 for shorter wavelengths. In this study, the daily-averaged Level 1.5 AERONET products, which are cloud-screened (Smirnov et al., 2000), were used in the period 19 to 25 February at six AERONET stations in south Asia [Solar Village (24.91N, 46.41E), Abu_Al_Baukhoosh (25N, 53E), Karachi (24N, 67E), MCO-Hanimaadhoo (6N, 73E), Pune (18N, 73E) and Kanpur (26N, 80E)], cited in an increasing longitude order.

2.2.4. LIDAR

A Portable Micro pulse Lidar system operating at 532 nm fabricated by the National Atmospheric Research Laboratory (NARL) is used in the present study (Kumar, 2006). The LIDAR system was operating in late-evening hours (post-sunset) under cloudless conditions. The LIDAR laser output pulse

energy is set at 10 μJ with 2500 Hz pulse repetition rate. The laser system bin width was set at 200 ns, corresponding to a height resolution of 30 m. The raw data profile was integrated every 2 minute interval, which corresponds to 3 lakhs shots integrated photon-count profile. The design specifications of portable lidar system are described elsewhere (Kumar, 2006). The lidar measures the height profile of backscattered signal from aerosols, during clear sky, which is converted into backscattering ratio (R). R is defined as:

$$R = (\beta_a + \beta_m) / \beta_m \quad (3)$$

Where β_a and β_m are the backscatter coefficients of aerosols and molecules, respectively. The aerosol-backscatter ratio from the lidar return is estimated using the inversion method (Fernald, 1984; Klett, 1981). The extinction coefficient k and the optical thickness at 532 nm (τ_{532}) are estimated from lidar data using the equations:

$$k = S_a * \beta_a \quad (4)$$

$$\tau_{532} = \int k(Z) dz \quad (5)$$

Where, z is the range between the laser source and the target (~ 7 km) and S_a is the extinction-to-backscatter ratio, the so-called lidar ratio (Chiang et al., 2007).

2.3 Model applications

2.3.1. MM5

The mesoscale model MM5 (<http://www.mmm.ucar.edu/mm5/>) is a limited-area, nonhydrostatic, terrain-following sigma-coordinate model designed to simulate or predict mesoscale atmospheric circulation. The model is supported by several pre- and post- processing programs, which are referred to as the MM5 modeling system. The MM5 modeling system has been developed at Penn State and National Center Atmospheric Research (NCAR) as a community mesoscale model with contributions from users worldwide. In the present study, the MM5-derived winds at 500 and 700 hPa were analysed to study the variations in wind speed over the region during the dust storm period. The MM5 has been extensively used in meteorological studies and detailed information about it can be found elsewhere (e.g., Kotroni and Lagouvardos, 2001).

2.3.2. DREAM

Several regional models for simulation and prediction of the atmospheric dust cycle have been developed in the past decade (Engelstaedter et al. 2006). These models are essential in complementing dust-related observations, trying to explain the dust cycle and predicting its impact on surface-level PMs. In this context, the Dust REgional Atmospheric Model (DREAM) has reached a level of delivering reliable operational dust forecasts capable of predicting the major dust events over the Mediterranean, Iberian Peninsula and East Asia (Nickovic et al., 2001). In its operational version, for each soil texture type, fractions of clay, small silt, large silt and sand are estimated assuming typical particle-size radii of 0.73, 6.1, 18 and 38 μm , respectively. After a long-range transport, only the first two types of particles are relevant for analysis since their lifetime is larger than 12 h. Recent understanding of dust-cloud microphysics and dust-radiation interactions (Pérez et al. 2006), from which climate- and weather-prediction models can benefit, requires a deeper knowledge on the dust-source processes, size distributions and optical properties. Currently, the monitoring systems include conventional surface observations operating in urban and rural areas, and remote-sensing systems. Deposition or surface concentration data involve close-to-ground characteristics of the dust process. The long-range transport of desert dust mainly takes place in the free troposphere (Mattis et al. 2002). Thus, sun photometers delivering spectrally-resolved column-integrated data in combination with lidars providing information on the vertical aerosol structure seem to be the most appropriate tools for model evaluation. A detailed description of the DREAM model can be found in Nickovic et al. (2001) and Pérez et al. (2006). The present study uses the DREAM images of dust load and concentration over East Asia (also including continental India) for the dust event period.

3. Results and discussion

3.1 Synoptic meteorological conditions

The atmospheric dynamics and the severe meteorological phenomena (such as cyclones and hurricanes) are strongly related to the aerosol loading and properties in the atmosphere (Badarinath et al., 2008). On the other hand, the occurrence of Sahara dust events over the Mediterranean are mainly driven by the intense cyclones called Sharav, south of the Atlas Mountains (Morocco), which are generated by the thermal contrast between cold Atlantic air and warm continental air that cross north Africa during spring and summer (Moulin et al., 1998). Therefore, several studies in this region (e.g., Meloni et al., 2008;

Kaskaoutis et al., 2008) have associated the strong dust events with the prevailing meteorological fields. Moreover, several studies (e.g. Krishnamurti et al., 1998) have highlighted the effect of the Inter Tropical Convergence Zone (ITCZ) in the aerosol field over AS and the Indian Ocean. To this respect, before analyzing the aerosol properties due to the dust storm in south Asia and AS, the synoptic meteorology over the region has to be examined.

A cold front originating from the Turkish highlands passed over the southern coasts of Saudi Arabia, Iran and Pakistan on 21st February 2008 and triggered an intense dust storm on 22 and 23 February over south Asia and AS. A couple of days earlier, the same cold front raised a dust storm over Jordan and Iraq, on 18th and 19th February. In order to examine the synoptic meteorology and the prevailing winds over the south Asian region during the intense dust storm, the MM5 derived winds at 500 and 700 hPa are analyzed. Figures 1a, b show the wind speed and direction at 500 and 700 hPa, respectively, on 22 February 2008 at 12:00 UTC (+05:30 LST). In both atmospheric levels the wind direction was a persistent westerly flow with high ($>30 \text{ ms}^{-1}$) above Iran and Pakistan and low intensities in the middle and south part of AS and Indian Ocean. Over the Indian subcontinent the wind field consisted of a westerly flow in the northwestern part (Thar Desert) progressively decreasing in magnitude and shifting to a northerly flow over central and south India. The general meteorological field associated with the strong west- to-east winds caused the mobilization, lifting and long-range transport of dust particles. The black area (no data) in Fig. 1b (700 hPa) is attributed to the elevated terrain and the high mountains (usually over 6000 m) over this region (Imalaia, Karakoram and Tibetan plateau).

There are few studies that examine on the possible relation between cyclone activity/low- pressure systems and dust storms (Evan et al., 2006; Badarinath et al., 2008; Kaskaoutis et al., 2008). The association of dust storms with low-pressure systems over the study region was also observed during 12-14 December, 2003, 26-29 April, 2006, 9-12 May, 2006, 6-9 March, 2008, 20-24 March, 2008, and 11-23 April, 2008 suggesting that low- pressure systems over the Bay of Bengal/Indian Ocean cause changes in the synoptic weather patterns leading to dust storm over the Persian Gulf, Arabian Peninsula and AS. The study of such meteorological dynamics and their association with intense atmospheric phenomena (e.g., dust storms) has not been well investigated over the region and constitutes a challenge for further research.

3.2 Satellite observations

Figure 2 shows the Terra-MODIS visible (true color) image on 22 and 23 February (a) as well as the False Color Composites (FCC) of both Terra and Aqua on 22 February (b) above south Asia. An intense dust load can be clearly seen in both figures mainly over western and northern AS and Pakistan. The thick dust plume on 22 February seems to attenuate also moving northeasterly on 23 February (Fig. 2a). A dust storm of similar magnitude affected the region during the first week of February 2008 (not shown). Winter dust storms are relatively rare compared to the large occurrence of dust storms during summer in this region. However, in 2008, a number of dust storms were initiated due to an extremely dry winter, which has lower soil moisture over the entire south Asia. Once the dust is raised its direction of transport depends on the prevailing wind flow (Fig. 1), which is constrained by the synoptic pressure systems. Over AS, dust is normally transported southwest due to the northeast trade winds, which blow towards the ITCZ lying in the southern Hemisphere during Austral summer (Krishnamurti et al., 1998; Nair et al., 2004). However, if a low-pressure system develops over AS or Bay of Bengal, then the dust is preferentially transported towards it. In the present case, the strong westerlies transport the dust from the Arabian Peninsula towards northern AS, Pakistan and western India.

The desert dust aerosols are, in the majority of the cases, detectable in VIS satellite images (Fig. 2a) particularly over ocean (note the better dust identification over AS). Nevertheless, since mineral-dust aerosols can have similar reflectivity to the desert surfaces it can be difficult to detect them over land. Thus, the upwind edges of the plume are not distinct and are in places difficult to differentiate from the underlying bright desert surfaces (desert areas in Arabia, Iran and Pakistan). A range of different sedimentary environments emits dust from the Middle East, Arabian Peninsula and Thar Desert; these have different mineral compositions, which, in turn, control the radiative properties of dust (Sokolik, 2002). However, dust reflectivity varies depending on its chemistry and can decrease significantly with increased iron concentration (Arimoto et al., 2002; Dubovik et al., 2002). Consequently red, or iron-rich dust have relatively low blue reflectivity and thereby lower contrast relative to surface reflectance, whereas white dust (composed by carbonates and quartz) have higher reflectance in the VIS and significantly higher contrast with respect to the underlying surface (Baddock et al., 2008).

The Terra- and Aqua-MODIS products (AOD_{550} , FM and α -Ångström in the spectral band 550-865 nm) before, during and after the dust event are shown in Figs 3a, b, c, respectively. The mean values are

averaged over the area (9-33 N_o, 49-78 E_o) including the entire AS, southern Iran, Pakistan, eastern Arabian Peninsula and western India. The vertical bars exhibit the standard deviation of the mean due to the spatial aerosol inhomogeneity. The Terra and Aqua values are similar, also exhibiting the same temporal variability. The mean MODIS-Terra AOD value is 0.383, while the respective Aqua one 0.374. As shown, the AOD₅₅₀ values increase progressively from 18 to 21 February, exhibiting very high value (~0.7) on 22 February (major intensity of the dust event). After that date the AOD₅₅₀ progressively decreases, but at a lower rate, since the thick dust layer emitted in the middle and upper atmosphere can stay over there for several days. Note also the absence of precipitation not favoring a wet aerosol deposition. The mean spatial-averaged AOD₅₅₀ value of ~0.7 from both sensors on 22 February indicates the intensity of the dust storm, since it is much higher from the mean AERONET AOD₅₀₀ value of 0.51 obtained in May (a month with major dust intensity) over Solar Village (Kambezidis and Kaskaoutis, 2008). The same researchers also found that AOD₅₀₀ values larger than 0.7 were rather rare over Saudi Arabia. The larger standard deviation on 22 February also indicates the significant spatial variability in aerosol load over the area caused by the intense dust event.

The FM values are rather low for both sensors (0.323 and 0.308 for Terra and Aqua, respectively) clearly indicating the dominance of coarse-mode aerosols over south Asia in the study period. The differences in the mean values between Terra and Aqua are larger than the respective for AOD₅₅₀, since the calculation of the FM fraction is not so accurate, having stronger dependence on changes in the aerosol field and surface reflectance (Levy et al., 2007). Even though both sensors give lower FM values on 22 February, they also exhibit a decreasing trend characteristic of the higher atmospheric abundance in coarse-mode particles during and after the dust storm. The standard deviations remain high on all days, thus highlighting the large spatial variation in the FM values due to the concurrent presence of different aerosol types over the area (natural and anthropogenic). The α -Ångström (550-865 nm) was calculated over the ocean, thus having a higher accuracy due to the use of the MODIS-ocean algorithm (Remer et al., 2002). As expected, $\alpha_{550-865}$ is continuously decreasing in the examined period due to the presence of dust over the AS region. No significant change in the sea-surface wind speed was found, which in part can affect the aerosol size and properties due to emission of sea-salt aerosols (Ramachandran, 2004). Thus, the strong decreasing rate in $\alpha_{550-865}$ values is attributed to the presence of dust above AS. Another significant remark is the close agreement between the $\alpha_{550-865}$ values of both MODIS sensors giving a confirmation to the computed results. The spatial averaged $\alpha_{550-865}$ values during and after the dust event (~0.55-0.65) are comparable in magnitude with the $\alpha_{443-865}$ presented near

the African coast in the Mediterranean Sea in the period 1998-2004 using SeaWiFS data (Antoine and Nobileau, 2006). On the other hand, the higher $\alpha_{550-865}$ values in the pre-dust period (>0.8) are in agreement with those found over the North Mediterranean coast, close to European countries.

The spatio-temporal variation of the AOD₅₅₀ values in the study region during the period of the intense dust storm is shown in Figs 4a for Terra and Aqua, respectively. The AOD₅₅₀ values are analyzed in the period 18-26 February 2008 according to latitude (9°- 33°N) as averaged values in the longitude area 49°- 78° E. These figures also show the latitudinal variation of the aerosol load over AS and the adjoining continental arid and semiarid regions. Both satellites show great consistency in the spatio-temporal AOD₅₅₀ distribution with a correlation coefficient ($r=0.861$). The larger differences between the two figures are depicted in the central part as well as and in the area defined as “dust in Persian Gulf”, where Aqua shows little higher AOD₅₅₀ values than Terra. Moreover the area defined as “dust in Indo Gangetic Plains” exhibits, in its larger values, a temporal delay of one day, with the maximum to occur on 23 February. Similar temporal delay in the AOD₅₅₀ values over Indo-Gangetic Plains (IGP) compared to the major dust event is also shown in Terra observations. More specifically, both figures show that in the beginning of the period (18-21 February) the AOD₅₅₀ values are relatively low (<0.4) except of a region (dust in Persian Gulf), where the longitude-averaged AODs show larger values. These values occurred on 20 February and are attributed to the presence of an intense dust storm over the Persian Gulf (27°– 30°N, 49°-52°E). This dust storm was also obvious from Terra/Aqua MODIS images and rather constitutes the first stage of the intense dust storm occurred two days later. The major dust storm (reaching AOD₅₅₀=1.8 in longitude-averaged values) occurred on 22 February in the area 24°-26°N. This area covers the northern AS and the coastal regions of Iran and Pakistan. Furthermore, in both figures a long tail of lower AOD₅₅₀ is presented on the same day. The highest of these values are depicted in the western AS and near to the Arabian coast. The longitude- averaged AOD₅₅₀ values for these latitudes are much lower due to the relative clear atmospheric conditions over the eastern AS for the same latitudes. Above 28°N the longitude-averaged AOD₅₅₀ values correspond to land pixels (mainly eastern Pakistan, northwestern India and IGP). The general southwest-northeast axis of the dust plume (Fig. 2) driven by winds of similar direction (Fig. 1), is revealed in Fig. 4 since the dust (larger AOD₅₅₀) is delayed for one day at the northeastern latitudes. Finally, in both figures a strong south-to-north AOD₅₅₀ gradient is highlighted. Such an AOD gradient, also influencing the radiative forcing of the area, is very common over AS and has been well established by several publications (Moorthy et al., 2005; Satheesh et al.,

2006a; Nair et al., 2008; Kalapureddy and Devara, 2008). The respective latitudinal-averaged figures do not give any additional information and for this reason they are not provided.

The respective spatio-temporal distribution of the FM values for Terra and Aqua MODIS sensors is shown in Figs 4b, respectively. As above, the FM corresponds to longitude-averaged values over the area 49°-78° E. Although the spatio-temporal distributions seem to be more complicated than the previous ones the correlation coefficient is a little higher ($r=0.897$) since large differences in FM values do not exist. In these figures the intense dust storm on 22 February cannot be clearly revealed. However, there is a general tendency for lower FM values (coarse-mode aerosols) during and after the dust event. The different algorithms used over land and ocean as well as the choice of the most appropriate aerosol model to characterize the atmospheric conditions (Levy et al., 2007), provide significant variability in FM values, which are smoothed over longitude. Even though, a strong south-to-north gradient of lower FM values is highlighted in Fig. 4b. Such lower FM or α -Ångström values in the northern part of the AS, indicating the presence of coarse-mode aerosols, have been also obtained in earlier studies (Satheesh et al., 2006a; Nair et al., 2008; Kalapureddy and Devara, 2008). These studies also showed greater contribution to the fine-mode aerosols near the Indian coast (southeastern part of the AS). This statement is also obvious in the present study viewing the high longitude-averaged FM values at the lower latitudes in the pre-dust period, which are attributed to the large FM values in the eastern part of AS and close to the Indian subcontinent.

MODIS is one of the most widely and successfully used sensors for the detection of dust plumes (Ichoku et al., 2004; Badarinath et al., 2007a; Kaskaoutis et al., 2008) and for improved identification of the dust sources (Bullard et al., 2008; Baddock et al., 2008). Figure 5(a-d) shows the spatial distribution of Terra-MODIS AOD₅₅₀ and FM values over south Asia on 22 and 23 February, the days with the major dust intensity. The typical AOD₅₅₀ in relatively clear conditions is <0.2 , while for turbid atmospheres >0.3 (Kaskaoutis et al., 2007a). The MODIS AOD₅₅₀ product suggests that the highest AOD₅₅₀ values are associated with the dust plumes (see Fig. 2) mainly in the northern and western part of the AS, the Persian Gulf, south Iran and Pakistan (Fig. 5a). The highest values (above 3.5) are depicted over Pakistan and the northern parts of AS and are comparable in magnitude with those presented in the thick dust layer covered Greece on 17 April 2005 (Kaskaoutis et al., 2008). On 23 February (Fig. 5b), the dust storm seems to be thinner, thus the lower AOD₅₅₀ values, while its higher intensity is presented in the northeastern latitudes compared to that on the previous day. This indicates the movement of the major

dust layer with the prevailing winds (Fig. 1) and a step-by-step deposition of the heavier particles. The weather synoptic systems that cause dust storms show that the dust events are often associated with cloud cover (Kaskaoutis et al., 2008; Baddock et al., 2008). Thus, some parts of Fig. 5, where clouds are present, are excluded by MODIS cloud mask MODIS algorithm (Levy et al., 2007). The FM values seem to be more appropriate to observe the dust spatial distribution and its influence on FM values than those presented in Fig. 5. Thus, low FM values are presented in north and west AS on 22 February (Fig. 5c) associated with the dust storm. On the next day (Fig. 5d), the low FM values, indicative of coarse-mode aerosols, are spread over an extended area in AS, mainly northeast, limiting the presence of large FM values of anthropogenic origin to the southeastern part of AS and close to the Indian coast. The very low FM values over the Thar Desert are attributed to the different aerosol model (dust model) used in the MODIS land algorithm.

Figure 6(a, b) shows the spatial distribution of the AI on 22 and 23 February 2008 as derived from AURA-OMI measurements. OMI-AI data show dust presence over the majority of the region, thus suggesting a widespread dust event. The AI clearly outlines the main dust plume, which occurred in the area surrounding the Persian Gulf, southern Iran, Pakistan, northern AS and western part of India. There is evidence that the higher AI values are attributed to the desert-dust aerosols, since much lower AI values are observed over regions with significant anthropogenic pollution (West Indian coast and IGP). Therefore, the elevated dust particles give signal to AI values in contrast to the anthropogenic absorbing aerosols (such as soot and black carbon), which are mainly within the boundary layer over urban sites in India (Satheesh et al., 2006b). Some wings of the intense dust plume are observed above the central part of India and can also affect Hyderabad. The AI was found to be well correlated with AOD at UV wavelengths in Thessaloniki, Greece (Koukouli et al., 2006) and Mongu, Zambia (Hsu et al., 1999) under biomass-burning events. In both figures, the higher values of AI are in qualitative agreement with those of AOD₅₅₀. Besides, further comparison of Fig. 6(a, b) with Fig. 6(a, b) indicates that the enhanced AI and AOD₅₅₀ values move towards the wind direction, which is in close agreement with MM5 results (Fig. 1). Thus, the larger AI values are depicted in the east on 23 February, mainly over Pakistan, Thar Desert and northwestern India, following the AOD₅₅₀ spatio-temporal distribution.

The AI maximum values of ~ 3.0 over central Pakistan is comparable in magnitude with the maximum OMI-AI values (~ 3.5) presented over Greece during an intense Saharan dust event (Kaskaoutis et al., 2008) and the climatological TOMS-AI values over Sahara (Alpert et al., 2004), but lower from the

OMI-AI values (~ 4 -5) during intense dust events in Australia (Baddock et al., 2008). Despite the fact that the main dust-source regions as well as the areas with the high desert-aerosol density are clearly identified by the present OMI observations. Some recent publications (Bullard et al., 2008; Baddock et al., 2008) have shown that the OMI-AI data are less able to define the dust-source locations with the same precision as can be achieved using the combination of outputs from the MODIS L1B algorithms, due to the relative coarse resolution of the OMI-AI ($0.25^\circ \times 0.25^\circ$) used in the current study. However, this investigation is beyond the scope of the present work.

The short-term nature of some dust events (approximately 1 day or even less) display some difficulties and possible biases associated with their detection at the time of satellite overpasses, typically one per day for polar-orbiting satellites. Therefore, some dust activity is possible to be missed due to the relative timing of overpass and dust emissions. Significant biases on this may also be caused by the cloud cover, which is often associated with the dust plumes. As a consequence, in some cases, the high-temporal resolution data from geostationary satellites can be more appropriate for the detection of such events. For a better view of the spatio-temporal variation of the dust plume, a time series of False Color Composite (FCC) derived from KALPANA-1 VHRR is analyzed for the first time over the Indian region. Figure 8 shows the FCC images for a 3-hr interval (06:00, 09:00 and 12:00 UTC) on 22 February and for 05:00 UTC on 23 February. In the morning hours of 22 February there is only a thin dust plume over north AS, Pakistan and west India, since the major dust layer was in the western AS. This dust layer was continuously increasing in thickness and moving northeast at noon and in early afternoon hours of 22 February. As the day progresses, the dust plume becomes more thick and spreads over an extended area affecting the northern and central parts of India (12:00 UTC). On 23 February the dust plume was continuously decreasing in thickness also moving eastward, while only some wings of the dust plume can be obvious from the FCC. From the KALPANA-1 VHRR images at higher temporal resolution (1-hr) it was calculated that the dust plume was transported towards the Indian subcontinent with a speed of $\sim 30 \text{ ms}^{-1}$.

Moreover, some interactions between elevated dust aerosols and clouds are shown over southern AS on 22 February, 12:00 UTC. Clouds also cover the northern part of Pakistan and the Imalaia region. The role and the effects of clouds in satellite retrievals are very important and great efforts have been made focusing on cloud-screening techniques (Kaufman et al., 2005). Proportionally to the thickness and the altitude of the clouds different effects (biases) in the dust detection can be revealed. Thus, the dense

cloud cover can obscure dust, while cirrus clouds, which have similar reflectance and brightness temperature difference (BTD) to fine dust aerosols (Baddock et al., 2008), can bias (probably overestimate) the dust presence. This is obvious in Fig. 7 since the desert- dust aerosols have similar reflectance and color with the cirrus clouds observed in the southern part of AS and above the mountains in northern Pakistan, India and Nepal. Note also (Fig. 5) that the MODIS algorithms did not give data over these regions on 22 and 23 February.

However, over bright and highly-reflected surfaces (e.g., desert regions and snow- covered areas), in the presence of clouds, during nighttime the aerosol detection using MODIS or TOMS/OMI can become increasingly uncertain (Levy et al., 2007; Torres et al., 2007). For this reason lidar systems on board satellites (such as CALIPSO) have been increasingly available in the last years. The CALIPSO-derived total attenuated backscatter at 532 nm and the Vertical Feature Mask (VFM) data products were used to identify the position of dust along the overpass trajectory. A typical example of the vertical distribution of the dust plume over the study region during daytime and nighttime on 22 February 2008 is shown in Fig. 8(a, b). Both figures show the overpass trajectory (moving northwards for daytime conditions and southwards for nighttime), the vertical profile of the total attenuated backscatter at 532 nm and the VFM image, which highlights the signals into 7 categories. The category 3 (aerosol, in orange) has a greater importance as well as the presence of clouds (cyan). In the lower part of both figures the coordinates of the overpass (latitude above and longitude below) are also given. The daytime pass of CALIPSO at 09:03 UTC (+05:30 LST) mainly covers a part of the Persian Gulf and nearly the entire AS, where the dust storm occurred. In addition, the nighttime pass of CALIPSO was at 20:56 UTC above AS and the western part of India (somewhat more to the east than the daytime pass). In both figures the presence of cirrus clouds is very limited, while low-altitude clouds mainly occurred over the mountains (elevated terrain, grey or black in VFM image).

The Fig. 8a shows a dust layer developed over the northeastern part of the AS extended from ground level to a height of 3–5 km. It should be noted that this is the highest altitude dust layer in the figure. Another dust layer at lower latitudes and higher longitudes (left part of the figure) is attributed to the combination of dust aerosols with anthropogenic pollution near the southwestern Indian coast. As regards the nighttime conditions (Fig. 8b), the dust layer is located in a more extended area, also covering the southeastern part of the AS (as has also been observed from Fig. 7). However, the most vertically-extended dust layer is confined at similar latitudes as before (even though a little to the north

for nighttime conditions). In contrast, this elevated dust layer has moved eastwards in the time interval of ~12 hrs between the two CALIPSO observations (~66°E and ~70°E for daytime and nighttime conditions, respectively). The mineral dust layer had high values of backscatter indicating that the layer was thick. It was also found that the depolarization

ratio was high because it was primarily composed of large non-spherical particles (Huang et al., 2007). The vertical profiles of total attenuated backscatter at 532 nm and VFM clearly show the vertical structures of the dust layers over the western part of India and AS at the same altitude (3-5 km) suggesting a long-range transport of dust aerosols (Liu et al., 2008). The location where the higher attenuated backscatter values are presented for the dust plume occurrence is in close agreement with MODIS AOD₅₅₀ and OMI-AI figures, while the movement of the dust plume to the east is consistent with the KALPANA-1 VHR images. These comparisons reveal the great importance of using the CALIPSO data for the identification of such events over the globe.

3.4 AERONET measurements

The CIMEL measurements at six AERONET stations located in the study area are examined in this section in order to reveal the spatio-temporal effect of the dust plume on the aerosol load and optical properties (Fig. 9). The stations are characteristic of different environments, such as continental areas at Arabian Peninsula and Persian Gulf (Solar Village, Abu_Al_Bukhoosh) directly affected by dust, urban areas in South Pakistan (Karachi) having both natural and anthropogenic emissions, stations in India (Pune and Kanpur) with significant amount of urban aerosols and MCO located in the southeastern AS with significant effect from urban-pollution transport from the Indian subcontinent. The colors were chosen in such a way in order to show the location of the stations according to longitude (i.e., violet-to-red for western-to-eastern stations). This can help in understanding the temporal variation of the aerosol properties directly controlled by the movement of the dust plume. The AOD₅₀₀ (Fig. 9a) shows higher values at the western stations on the first days and lower afterwards; when on the contrary, the AOD₅₀₀ increased on 22 February in the eastern stations, directly affected by the dust storm. This fact verifies the aforementioned statement that the dust storm was above the Arabian Peninsula and Persian Gulf two days before, but with a low intensity. The highest AOD₅₀₀ is observed over Kanpur and Karachi (measurements only on 23 February) due to the combined effect of natural (desert dust) and anthropogenic aerosols. The different environments divide the six stations into two groups regarding the

$\alpha_{440-870}$ values (Fig. 9b). The stations with significant contribution of anthropogenic aerosols present much higher $\alpha_{440-870}$ values (>1.0) compared to the rest (<0.5). The temporal variation of the $\alpha_{440-870}$ values is somewhat similar to that of AOD_{500} . Thus, the western stations exhibit lower values on 21 February, just after the passage of the dust storm over their locations, while the eastern stations present lower $\alpha_{440-870}$ values in the end of the period, since the dust plume affects those 2 days later.

The dominant aerosol types (coarse- and fine-mode) can easily be defined in Fig. 9c, where the coefficient a_2 from the second-order polynomial in the $\ln AOD$ vs $\ln \lambda$ values ($\ln AOD = a_2 \ln \lambda^2 + a_1 \ln \lambda + a_0$) is analyzed. This coefficient shows the curvature and can further be used for the discrimination of the different aerosol types (Eck et al., 1999; Kaskaoutis et al., 2007b). The almost zero or positive values show a significant contribution of the coarse-mode aerosols, while the negative ones are characteristic for the presence of fine-mode aerosols. The very large values for Pune in 18-19 February are composed by large uncertainties while in all the other cases the polynomial fit was accurate ($R^2 > 0.98$). This coefficient seems not to have great effect from the dust plume, especially for the coarse-mode aerosols. On the other hand, there is a tendency for higher (less negative) a_2 values for the fine-aerosol dominated stations. This indicates higher contribution of coarse-mode aerosols in the atmospheric column on the last days probably affected by the presence of dust. The temporal variation of the fine-mode fraction (Fig. 9d) is similar to that of $\alpha_{440-870}$, further verifying the eastwards movement of the dust plume. A general statement that can be revealed from Fig. 9 is that the variation in aerosol load and properties is more pronounced at continental stations without influences of local anthropogenic sources. In such areas the natural sources (dust storms or biomass burning) affect more intensely the aerosol field in the vertical (Kambezidis and Kaskaoutis 2008).

3.5 DREAM predictions

The DREAM images during the dust event are also provided (Fig. 10) in order to show the spatial distribution of the dust load ($g\ m^{-2}$) and concentration ($\mu g\ m^{-3}$). The DREAM model focuses its predictions above and near the major dust-source regions (Sahara/Sahel and East Asian deserts). Therefore, its coverage over the study region is limited to including Pakistan and continental India. The DREAM images are provided for 21, 22 and 23 February at 12:00 UTC. Both dust load and concentration over Pakistan and India seems to be larger on 21 February continuously decreasing on the other two days. This is opposite to the satellite and AERONET results presented above, which show

major intensity of the dust plume on 22 and 23 February. The DREAM model shows large dust load and concentration over Taklamakan desert in western China. Since the major dust sources in east Asia are displayed in western China and Mongolia the model is mainly specified at these areas as well as the whole Mediterranean basin; over these regions the DREAM predictions seem to be in close agreement with lidar and AERONET measurements (Pérez et al. 2006). This may be the main reason for the relative inability of the model to predict the dust intensity and spatio-temporal distribution above south Asia. However, the model clearly shows the dust presence over Pakistan and western India and can constitute a useful tool in monitoring dust outbreaks from the Thar Desert.

3.6 Lidar measurements in Hyderabad

Both satellite sensors and sun photometers measure the columnar aerosol properties without providing any information about the vertical structure of the aerosols. However, in many cases the surface aerosol properties may be different from columnar aerosol ones because of the presence of distinct aerosol layers above (Ramanathan et al., 2001; Satheesh et al., 2006b). Such vertical aerosol layers may occur as a consequence of strong thermal convection, which lifts aerosols from ground to greater heights. It could also occur due to the long-range aerosol transport (Pérez et al. 2006). Therefore, knowledge of the vertical distribution of the aerosols in the atmosphere is important in estimating its radiative forcing (Kinne and Poeschel, 2001). The information on the vertical aerosol distribution is sparse over India. There exist a few studies on the vertical distribution of aerosols using aircraft-based measurements (Moorthy et al., 2004; Tripathi et al., 2005). More recently, Satheesh et al. (2006b) found that the winter aerosol-lidar profile was extended to higher altitudes than the summer one at the urban continental station of Bangalore, near Hyderabad. The present work is among the very first studies using vertical aerosol profiles over Hyderabad during dust storm period.

In this section the vertical distribution of aerosols over the urban location of Hyderabad in central India, is examined using a lidar system and the effects of the boundary layer dynamics and the long-range dust transport above it are deduced. Figure 11 shows the lidar-derived aerosol backscatter profile at 532 nm on 22 and 23 February 2008, those two days that were affected by the long-range dust transport. The time shown is Indian Standard Time (IST). The lidar measurements started in the evening (~18:30) on 22 February and continued till early morning of 23 February (~06:00). Nighttime and early morning hours are characterized by a shallow layer of anthropogenic aerosols, a few hundred meters thick.

During nighttime the rapid cooling of the Earth's surface leads to the formation of the nocturnal stable layer, trapping the aerosols into it. As day advances, the strong convective eddies are seen to diffuse the aerosols vertically up to more than 1.5 km. As expected, the majority of the aerosols are confined to a shallow layer (~1 km), especially in the early morning hours of 23 February, when the aerosol load near the ground starts to increase due to anthropogenic activities. In the night hours (23:00-03:00) the near-surface aerosols are significantly lower due to decrease in anthropogenic activities and emissions. In the evening hours of 22 February the aerosol profile shows the presence of a strong turbulent mixing, lifting the aerosols upwards. Thus, the aerosol layer deepens significantly to reach as high as about 2 km (from >1 km at night).

Despite the boundary-layer aerosols, an elevated aerosol layer (~3 km) is observed above them suggesting long-range transport of dust aerosols, influencing Hyderabad at midday of 22 February (not shown). The plume-like structure of increased aerosol concentration is visible above the boundary layer aerosols extending up to 3 km. The vertical extent of the dust aerosols over Hyderabad is in general agreement with the Sahara dust transport over Spain (Pérez et al. 2006) and Atlantic (McConnell et al., 2008), mainly being formed between 2 and 4 km. The information on the physical properties of boundary-layer aerosols and free-troposphere ones can be derived using lidar measurements.

3.7 Solar radiation measurements in Hyderabad

Surface solar irradiance measurements were also carried out in the tropical urban region of Hyderabad, India, to examine the effects of the long-range transport of dust aerosols. Figure 12 shows the day-to-day variation of AOD₅₀₀ and α -Ångström before, during and after the dust-plume passage (18-25 February 2008). It should be mentioned that no data were available on 24 February due to an extended cloud cover over the area. The AODs were obtained from the MICROTOPS-II sun photometer in a time interval of 30 min, starting at ~09:00 and ending at 17:00 IST. The α -Ångström was calculated in the spectral band 440-870 nm ($\alpha_{440-870}$), using the least-squares technique, in order to be comparable with that of the AERONET stations; this calculation method has recently been established as the least imprecise and wavelength-dependent (Kaskaoutis and Kambezidis 2008). The AOD₅₀₀ presents very large values, often above 0.8, exhibiting a mean value of 0.783 ± 0.242 indicative of very turbid conditions over Hyderabad. These values are higher than previous ones in the same area (Latha and

Badarinath, 2005b; Badarinath et al., 2007b), as well as those presented over four AERONET sites (Kambezidis and Kaskaoutis, 2008) or over urban Athens (Kaskaoutis et al., 2006).

On certain occasions the AOD₅₀₀ takes extremely high values (highlighted as dust events in the figure). Two of these events are presented on 22 February, when the dust plume affects Hyderabad area. On that day the dust plume also affected the AERONET stations (Fig. 9) in continental India (Pune and Kanpur), which are located at similar to Hyderabad longitudes. Such high AOD values have also been observed over Hyderabad during the dust event of 10 April 2006 (Badarinath et al., 2007a). However, the peaks in AOD₅₀₀ on certain occasions may be contaminated by thin cirrus clouds at the measurement time, undetected with naked eye. The $\alpha_{440-870}$ has a mean value of 1.019 ± 0.194 exhibiting a trend for lower values on 22 and 23 February (daily mean of 0.89 and 0.92, respectively), during and after the dust-plume passage. Moreover, the peaks in AOD₅₀₀ are associated with gaps in $\alpha_{440-870}$ values, further indicating that the larger AODs are mainly attributed to enhanced aerosol load composed of coarse-mode particles. Similar α values, with and without dust, were observed over Hyderabad during the dust event of 10 April 2006 (Badarinath et al., 2007a). Comparing the $\alpha_{440-870}$ values in Hyderabad with those at the six AERONET sites (Fig. 9), it is concluded that the Hyderabad site exhibits aerosol characteristics between the two groups revealed in Fig. 10, indicating a rather mixed aerosol type under very turbid conditions.

The scatter plot of AOD₅₀₀ vs $\alpha_{440-870}$ can be used for the identification of different aerosol types (El-Metwally et al., 2008). The same plot is performed for the study period (18-25 February) over Hyderabad (Fig. 13). From the AOD₅₀₀ vs $\alpha_{440-870}$ diagram dust and anthropogenic aerosols can be identified over Hyderabad. Note that the dust aerosols are mainly detected on the last days (22 and 23 February), while the anthropogenic ones on the first days of the study period. However, the combined effects of both natural and anthropogenic aerosols over the region result in a rather mixed-aerosol type as regards the daily mean values, according to the suggestions by Pace et al. (2006) and Kaskaoutis et al. (2007b).

In India, efforts have been made to study the aerosol behavior and their interaction with solar radiation in some urban cities establishing a network of seven stations (including Hyderabad) under the Indian Space Research Organization Geosphere Biosphere Program (ISRO-GBP), where a multi-wavelength solar radiometer is deployed (Moorthy et al., 1999). Using the organized network of ground-based

instruments at Hyderabad actinometric station, the solar irradiance attenuation can further be investigated on 22 and 23 February 2008. Figure 14 shows the MFRSR measured variations in the three components (global, diffuse and direct-beam) of solar irradiance (400–1100 nm) on 22 and 23 February. The black color corresponds to 22 while the red to 23 February. A significant reduction in direct-beam irradiance started after 15:00 LST on 22 February (the black curves are much lower than the red ones) and continued up to 11:00 LST on 23 February (the red curves are lower than the black ones). Similarly, reduction in global solar irradiance occurred in this time interval associated with an increase in diffuse component. The higher aerosol loading due to the dust-plume passage over Hyderabad at these hours seems to have a great influence on the amounts of solar radiation at ground level. In the time interval of the intense dust-plume event over Hyderabad (14:00-17:00 LST on 22 February) the reduction in global solar irradiance was calculated to 11.6%, while that in direct-beam to 41.7%. In contrast, the diffuse radiation increased 24% in this time interval, compared to that without dust over the area. Moreover, PM₁₀ concentrations measured by a high-volume sampler also showed ~50% increase for the same time period. It should be noticed that the change in solar irradiance components in the morning hours of 23 February can partly be attributed to the enhanced aerosols in the boundary layer (Fig. 11). However, despite the thick aerosol layer near the surface, the dust plume is also apparent at this time over Hyderabad.

The changes in solar irradiance due to the additional aerosol loading are further investigated through the diffuse-to-direct-beam ratio (DDR) on 22 and 23 February. The diurnal spectral variation of DDR is shown in Fig. 15 for the six MFRSR wavelengths. DDR has been established to constitute a useful parameter in estimating atmospheric optical properties, such as optical depths and light absorption index (King, 1979). DDR is also sensitive to aerosol loading and single scattering albedo and has been used to distinguish aerosols in respect of their origin (e.g. desert dust and biomass smoke) in Mediterranean (Meloni et al., 2006). More recent studies (e.g. Kaskaoutis et al., 2007c) have shown that DDR can constitute a powerful tool for monitoring atmospheric turbidity. These studies have shown that as the wavelength increases the DDR has negligible effect on the solar zenith angle and, thus, it can be assumed that DDR depends only on atmospheric turbidity. DDR has already been used over Hyderabad in order to identify the dust event of 10 April 2006 (Badarinath et al., 2007a). It is clearly shown that the DDR values are higher on 22 February (black) after midday when the dust load affects the study area. In the morning hours of 23 February DDR is larger than the respective of 22 February, as has previously observed in the solar irradiance and AOD₅₀₀ measurements. In general, the diurnal variation of DDR

exhibits similar plot for all wavelengths. The differences are depicted in late afternoon, where the DDR increases at the shorter wavelengths only. This increase is attributed to the effect of solar zenith angle and not to an increase in turbidity levels, an effect that is diminished at the longer wavelengths (Kaskaoutis et al., 2007c).

4. Conclusions

In the present study a wintertime intense dust storm occurred in south Asia (including Persian Gulf, Arabian Sea and western India), was investigated via remote-sensing observations and ground-based measurements. Several satellite observations from sensors such as MODIS on board Terra and Aqua, OMI on board AURA, CALIPSO and KALPANA-1 VHRR were used to detect the main source regions of the dust outbreak and monitor its spatio-temporal variation. Additionally, AERONET measurements over six stations in south Asia as well as MICROTOSPS-II and MFRSR measurements over Hyderabad, India, accomplished and partially validated the satellite observations. Finally, the models MM5 and DREAM were used to provide the meteorological fields favoring the desert-dust emission and the spatio-temporal distribution of the dust load and concentration, respectively.

Strong winds, both in surface and middle troposphere, favored the exposure, uplift and long-range transport of desert-dust aerosols covering an extended area of the Persian Gulf, AS, Pakistan and western India. The prevailing wind direction was southwest-to-northeast, transporting the dust plume eastwards. The areas in the Persian Gulf were affected by the dust plume one or two days before its major intensity, which occurred on 22 February, while locations in continental India one day after. Both MODIS and OMI observations identified aerosols in Pakistan, where the dust plume presented its highest intensity. All the satellite sensors showed an eastward movement of the dust plume. Significant contribution was offered by the KALPANA-1 geostationary satellite, which provided a unique opportunity to monitor the transport of dust aerosols over the Indian region. The AOD values associated with the dust event were very high and comparable to those of other intense dust storms worldwide. Lidar measurements over Hyderabad revealed an elevated aerosol layer (~3 km) above the thick boundary aerosol layer, thus giving very large AOD₅₀₀ values (above 1.0) on certain occasions during the dust event. The dust presence over Hyderabad in the afternoon hours of 22 February caused a significant decrease in global and direct-beam irradiances with a concurrent increase of the diffuse component.

The combined use of satellite sensors with sun photometer measurements, regional dust models and lidar systems, sounds very appropriate for the dust transport investigation. The improvement of the knowledge about the dust-source regions, the transport pathways, the seasonality of the dust storms and their optical characteristics above south Asia and AS must be further achieved by a combination of in-situ and remote-sensing measurements and experimental campaigns. Since the contribution of dust to the total atmospheric aerosol load is significant, future efforts in examining the global climate could focus their main efforts on understanding the role of dust in the climate system.

Acknowledgements

The authors thank the Director of NRSC & Dy. Director (RS&GIS-AA), NRSC for necessary help at various stages and ISRO-GBP for financial support. The authors also thank the principal investigators for their effort in establishing and maintaining the AERONET stations used in the study (Dr Brent Holben, Dr Giuseppe Zibordi, Dr Naif Al-Abbadi, Dr Panuganti C. S. Devara, Dr S. N. Tripathi and Prof. V. Ramanathan). The authors would like to thank the MODIS and OMI science data support team (past and present) for processing data via the Giovanni website (<http://giovanni.gsfc.nasa.gov/>) as well as the KALPANA and CALIPSO scientific teams. The scientists who developed and are operating the DREAM and MM5 models are also gratefully acknowledged.

References

- Ahmad, S. P., Levelt, P. F. Bhartia, P. K. Hilsenrath, E. Leppelmeier, G.W. and Johnson, J. E. 2003. Atmospheric Products from the Ozone Monitoring Instrument (OMI), *Proceedings of SPIE conference on Earth Observing Systems VIII*, 5151, 619630. (http://acdisc.gsfc.nasa.gov/ozone/docs/omispie_2003.doc).
- Alpert, P., Kishcha, P., Shtivelman, A., Krichak, S. O., Joseph, J. H., 2004. Vertical 22 distribution of Saharan dust based on 2.5-year model Predictions, *Atmos. Res.* 70, 109- 130.
- Antoine, D. and Nobileau, D., 2006. Recent increase of Saharan dust transport over the Mediterranean Sea, as revealed from ocean color satellite (SeaWiFS) observations, *J. Geophys. Res.* 111, D12214, doi:10.1029/2005JD006795.
- Arimoto, R., Balsam, W. and Schloesslin, C., 2002. Visible spectroscopy of aerosol particles collected on filters: iron-oxide minerals, *Atmospheric Environment*, 36, 89-96.
- Astitha, M., Kallos, G. and Katsafados, P., 2008. Air pollution modelling in the Mediterranean Region: Analysis and forecasting of episodes, *Atmos. Res.*, 89, 358-364.

Badarinath, K. V. S., Kharol, S. K., Kaskaoutis, D. G. and Kambezidis, H. D., 2007a. Case study of dust storm over Hyderabad area, India: Its impact on solar radiation using satellite data and ground measurements, *Science of the Total Environment*, 384, 316-332.

Badarinath, K.V.S., Kharol, S. K., Kaskaoutis, D. G. and Kambezidis, H. D., 2007b. Influence of atmospheric aerosols on solar spectral irradiance in an urban area, *J. Atmos. Sol. Terr. Phys.* 69, 589-599.

Badarinath, K.V.S., Kharol, S. K., Kiran Chand, T. R., Parvathi, Y. G., Anasuya, T. and Jyothsna, A. N., 2007c. Variations in black carbon aerosol, carbon monoxide and ozone over an urban area of Hyderabad, India, during the forest fire season, *Atmospheric Research*, 85, 18-26.

Badarinath, K.V.S., Kharol, S. K., Krishna Prasad, V., Kaskaoutis, D. G. and Kambezidis, H. D., 2008. Variation in aerosol properties over Hyderabad, India during intense cyclonic conditions, *Intern. J. Remote Sensing*, 29, 4575-4597.

Baddock, M.C., Bullard, J. E. and Bryant, R. G., 2008. Dust source identification: a comparison of techniques, *Rem. Sensing of Environment* (accepted for publication).

Bhattacharya, B. K., Mallick, K., Nigam, R., Patel, N. K., Padmanabhan, N., Mahammad, S. S., Ramakrishnan, R. and Parihar, J. S., 2008. A study on Land Surface Radiation Budget Parameters using KALPANA-1 and INSAT 3A CCD data for Agrometeorological Applications, ISRO/ASP/SAC/01/2008, pp 1 – 44.

Bullard, J. E., Baddock, M. C., McTainsh, G. H. and Leys, J. F., 2008. Sub-basin scale dust source geomorphology detected using MODIS, *Geophysical Research Letters*, doi:2008GL033928.

Chiang, C. W., Chena, W. N., Liangb, W. A., Dasb, S. K. and Neeb, J. B., 2007. Optical properties of tropospheric aerosols based on measurements of lidar, sun-photometer, and visibility at Chung-Li (251N, 1211E), *Atmospheric Environment*, 41, 4128–4137.

Colette, A., Menut, L., Haeffelin, M. and Morille, Y., 2008. Impact of the transport of aerosols from the free troposphere towards the boundary layer on the air quality in the Paris area, *Atmospheric Environment*, 42, 390-402.

Donaghay, P. L., Liss, P. S., Duce, R. A., Kester, D. R., Hanson, A. K., Villareal, T., Tindale, N. W. and Gifford, D. J., 1991. The role of episodic atmospheric nutrient inputs in the chemical and biological ecosystems, *Oceanography* 4, 62-70.

Dubovik, O., Smirnov, A., Holben, B. N., King, M. D., Kaufman, Y. J., Eck, T. F. and Slutsker, I., 2000. Accuracy assessments of aerosol properties retrieved from Aerosol Robotic Network (AERONET) sun and sky radiance measurements, *J. Geophys. Res.* 105, 9791-9806.

Dubovik, O., Holben, B. N., Eck, T. F., Smirnov, A., Kaufman, Y. J., King, M. D., Tanrè, D. and Slutsker, I., 2002. Variability of absorption and optical properties of key aerosol types observed in worldwide locations, *J. Atmos. Sci.* 59: 590-608.

Dust Storms, Sand Storms and related NOAA Activities In The Middle East, NOAA magazine online story 86, April, 2003.

Eck, T. F., Holben, B. N., Reid, J. S., Dubovic, O., Smirnov, A., O' Neill, N. T., Slutsker, I. and Kinne, S., 1999. Wavelength dependence of the optical depth of biomass burning, urban, and desert dust aerosols, *J. Geoph. Res.* 104, D24, 31333-31349.

Eck, T. F., Holben, B. N., Ward, D. E., Dubovic, O., Reid, J. S., Smirnov, A., Mukelabai, M. M., Hsu, N. C., O' Neil, N. T. and Slutsker, I. 2001. Characterization of the optical properties of biomass burning aerosols in Zambia during the 1997 ZIBBEE field campaign, *J. Geoph. Res.* 106, D4, 3425-3448.

El-Askary, H., Gautam, R., Singh, R. P. and Kafatos, M., 2006. Dust storms detection over the Indo-Gangetic basin using multi sensor data, *Advances in Space Research*, 37 (4), 728-733. El-Metwally, M., Alfaro, S. C., Abdel Wahab, M. and Chatenet, B., 2008. Aerosol characteristics over urban Cairo: Seasonal variations as retrieved from Sun photometer, *J. Geophys. Res.*, 113, D14219, doi:10.1029/2008JD009834.

Engelstaedter, S., Tegen, I. and Washington, R., 2006. North African dust emissions and transport, *Earth-Science Reviews* 79: 73-100.

Evan, A. T., Heidinger, A. K. and Pavolonis, M. J., 2006. Development of a new over- water Advanced Very high Resolution Radiometer dust detection algorithm, *International Journal of Remote Sensing*, 27 (18), 3903- 3924. doi:10.1080/01431160600646359.

Fernald, F. G., 1984. Analysis of atmospheric lidar observations: some comments, *Applied Optics*, 23(5), 652-653.

Goudie, A. S. and Middleton, N. J., 2001. Saharan dust storms: nature and consequences, *Earth-Science Reviews* 56: 179-204.

Griffin, D.W., Kellogg, C. A., Garrison, V. H., Lisle, J. T., Borden, T. C. and Shinn, E. A., 2003. Atmospheric microbiology in the northern Caribbean during African dust events, *Aerobiologia* 19, 143–157.

Habib, G., Venkataraman, C., Chiapello, I., Ramachadran, S., Bopucher, O. and Reddy, M. S., 2006. Seasonal and interannual variability in absorbing aerosols over India derived from TOMS: Relationship to regional meteorology and emissions, *Atmos. Envir.* 40, 1909-1921.

Harrison, L., Michalsky, J. and Derndt, J., 1994. Automated Multifilter rotating shado- band radiometer: an instrument for optical depth and radiation measurements, *Applied Optics* 33, (22) 5118-5125.

Harrison, S. P., Kohfeld, K. E., Roelandt, C. and Claquin, T., 2001. The role of dust in climate changes today, at the last glacial maximum and in future, *Earth-Science Reviews*, 54,1-3, 43-80.

Holben, B. N., Tanre, D., Smirnov, A., Eck, T. F., Slutsker, I. et al., 2001. An emerging ground-based aerosol climatology: Aerosol optical depth from AERONET, *J. Geophys. Res.* 106, 12,067-12,097.

Hsu, N. C., Herman, J. R., Torres, O., Holben, B. N., Tanre, D., Eck, T. F., Smirnov, A., Chatenet, B. and Lavenu, F., 1999. Comparisons of the TOMS aerosol index with sunphotometer aerosol optical thickness: Results and applications, *J. Geophys. Res.* 104, 6269-6279.

Huang, J., Lin, B., Minnis, P., Wang, T., Wang, X., Hu, Y., Yi, Y. and Ayers, J. K., 2006. Satellite-based assessment of possible dust aerosols semidirect effect on cloud water path over East Asia, *Geophys. Res. Lett.*, 33, L19802, doi:10.1029/2006GL026561.

Huang, J., Minnis, P., Yi, Y., Tang, Q., Wang, X., Hu, Y., Liu, Z., Ayer, K., Trepte, C. and Winker, D., 2007. Summer dust aerosols detected from CALIPSO over the Tibetan Plateau. *Geophysical Research Letters*, VOL. 34, L18805, doi:10.1029/2007GL029938, 2007.

Ichoku, C., Kaufman, Y. J., Remer, L. A. and Levy, R., 2004. Global aerosol remote sensing from MODIS, *Advances in Space Research*, 34, 820-827.

Kalapureddy, M. C. R. and Devara, P. C. S., 2008. Characterization of aerosols over oceanic regions around India during pre-monsoon 2006, *Atmos. Environ.*, 42, 6816-6827, doi:10.1016/j.atmosenv.2008.05.022.

Kambezidis, H. D. and Kaskaoutis, D.G., 2008. Aerosol climatology over four AERONET sites: An overview, *Atmospheric Environment*, 42, 1892-1906.

Kaskaoutis, D. G., Kambezidis, H. D., Adamopoulos, A. D. and Kassomenos, P. A., 2006. On the determination of aerosols using the Ångström exponent in the Athens area, *J. Atmos. Solar Terr. Phys.*, 68, 2147-2143.

Kaskaoutis, D.G., Kosmopoulos, P., Kambezidis, H. D. and Nastos, P. T., 2007a. Aerosol climatology and discrimination of different types over Athens, Greece based on MODIS data. *Atmos. Environ.* 41, 7315-7329.

Kaskaoutis, D. G., Kambezidis, H. D., Hatzianastassiou, N., Kosmopoulos, P. G. and Badarinath, K. V. S., 2007b. Aerosol climatology: dependence of the Angstrom exponent on wavelength over four AERONET sites, *Atmosph. Chem. Phys. Discuss.*, 7, 7347-7397, <http://www.atmos-chem-phys-discuss.net/7/7347/2007/>.

Kaskaoutis, D. G., Kambezidis, H. D. and Tóth, Z., 2007c. Investigation about the dependence of spectral diffuse-to-direct-beam ratio on atmospheric turbidity and solar zenith angle, *Theoretical and Applied Climatology*, 89, 245-256.

Kaskaoutis, D. G. and Kambezidis, H. D., 2008. Comparison of the Ångström parameters retrieval in different spectral ranges with the use of different techniques, *Meteorol. Atmos. Phys.*, 99, 233-246.

Kaskaoutis, D.G., Kambezidis, H. D., Nastos, P. T. and Kosmopoulos, P. G., 2008. Study on an intense dust storm over Greece, *Atmospheric Environment*, 42, 6884-6896.

Kaufman, Y. J. and Tanrè, D., 1998. Algorithm for remote sensing of tropospheric aerosol from MODIS, *Algorithm Theoretical Basis Documents (ATBD-MOD-02)*, PP. 85.

Kaufman, Y. J., Tanrè, D. and Boucher, O., 2002. A satellite view of aerosols in the climate system, *Nature*, 419, 215–23.

Kaufman, Y. J., Remer, L. A., Tanrè, D., Li, R-R., Kleidman, R., Mattoo, S., Levy, R. C., Eck, T. F., Holben, B. N., Ichoku, C., Martins, V. J. and Koren, I., 2005. A Critical examination of the residual cloud contamination and diurnal sampling effects on MODIS estimates of aerosol over Ocean, *IEEE, Transactions on Geosci. and Remote Sens.*, 43, 2886-2897.

Kharol, S. K., and Badarinath, K. V. S., 2006. Impact of biomass burning on aerosol properties over tropical urban region of Hyderabad, India, *Geophysical Research Letters*, 33, L20801, doi: 10.1029/2006GL026759, 2006.

Kharol, S. K. and Badarinath, K. V. S., 2007. Effect of synoptic meteorological conditions on aerosol properties over urban environment: A study over tropical urban region of Hyderabad, India, *Acta Geophysica*, doi: 10.2478/s11600-007-0009-3.

Kim, S. W., Yoon, S. C., Kim, J. and Kim, S. Y., 2007. Seasonal and monthly variations of columnar aerosol optical properties over east Asia determined from multi-year MODIS, LIDAR, and AERONET Sun/sky radiometer measurements, *Atmos. Envir.*, 41, 1634-1651.

King, M. D. 1979. Determination of the ground albedo and the index of absorption of atmospheric particulates by remote sensing. Part II: Application, *J.Atmos.Sci.* 36, 1072- 1083.

Kinne, S. and Pueschel, R., 2001. Aerosol radiative forcing for Asian continental outflow. *Atmos. Envir.* 35, 5019-5028.

Klett, J. D. 1981. Stable analytical inversion solution for processing lidar returns, *Applied Optics*, 20(2), 211-220.

Kotroni, V. and Lagouvardos, K., 2001. Precipitation forecast skill of different convective parameterization and microphysical schemes: application for the cold season over Greece, *Geophysical Research Letters*, 20, 10, 1977-1980.

Koukouli, M. E., Balis, D. S., Amiridis, V., Kazadsis, S., Bais, A., Nickovic, S. and Torres, O., 2006. Aerosol variability over Thessaloniki using ground based remote sensing observations and the TOMS aerosol index, *Atmos. Environ.* 40, 5367-5378.

Krishnamurti, T. N., Jha, B., Prospero, J., Jayaraman, A. and Ramanathan, V., 1998. Aerosol and pollutant transport and their impact on radiative forcing over the tropical Indian Ocean during the January-February 1996 pre-INDOEX cruise, *Tellus*, 50B, 521- 542.

Kumar, Y. B., 2006. Portable lidar system for atmospheric boundary layer measurements, *Optical Engineering*, 45(7), 076201.

Latha, K. M. and Badarinath, K. V. S., 2005a. Seasonal variations of black carbon aerosols and total aerosol mass concentrations over urban environment in India, *Atmospheric Environment*, 39 (22), 4129-4141.

Latha, K. M. and Badarinath, K. V. S., 2005b. Spectral solar attenuation due to aerosol loading over an urban area in India, *Atmos. Res.* 75, 257-266.

Lenes, J. M., Darrow, B. P., Cattrall, C., Heil, C. A., Callahan, M., Vargo, G. A., Byrne, R. H., Prospero, J. M., Bates, D. E., Fanning, K. A. and Walsh, J. J., 2001. Iron fertilization and the Trichodesmium response on the West Florida shelf. *Limnology and Oceanography* 46 (6), 1261–1277.

Levin, Z. and Ganor, E., 1996. The effects of desert particles on cloud and rain formation in the Eastern Mediterranean. In *The Impact of Desert Dust Across the Mediterranean*, Edited by S. Guerzoni and R. Chester, pp. 77-86, Springer, New York.

Levy, R. C., Remer, L. A., Tanre, D., Kaufman, Y. J., Ichoku, C., Holben, B. N., Livingston, J., Russell, P. and Mating, H., 2003. Evaluation of the MODIS retrievals of dust aerosol over the ocean during PRIDE, *J. Geoph. Res.* 108, doi:10.1029/2002JD002460.

Levy, R. C., Remer, L. A., Mattoo, S., Vermote, E. and Kaufman, Y. J., 2007. Second- generation operational algorithm: Retrieval of aerosol properties over land from inversion of Moderate Resolution Imaging Spectroradiometer spectral reflectance, *J. Geophys. Res.*, 112, D13211, doi:10.1029/2006JD007811.

Liu, Z., Omar, A., Vaughan, M., Hair, J., Kittaka, C., Hu, Y., Powell, K., Trepte, C., Winker, D., Hostetler, C., Ferrare, R., and Pierce, R., 2008. CALIPSO lidar observations

of the optical properties of Saharan dust: A case study of long-range transport, *Journal Of Geophysical Research*, Vol. 113, D07207, doi:10.1029/2007JD008878, 2008.

Mackie, D. S., Boyd, P. W., McTainsh, G. H., Tindale, N. W., Westberry, T. K. and Hunter, K. A., 2008. Biogeochemistry of iron in Australian dust: from eolian uplift to marine uptake, *Geochemistry ,Geophysics,Geosystemw*.9,doi:10.1029/2007GC001813

McConnell, C. L., Highwood, E. J., Coe, H. et al., 2008. Seasonal variations of the physical and optical characteristics of Saharan dust: Results from the Dust Outflow and Deposition to the Ocean (DODO) experiment, *J. Geophys. Res.*, 113, D14S05, doi:10.1029/2007JD009606.

McKinnon, D. J., Chavez, P. S., Fraser, R. S. Jr., Niemeyer, T. C. and Gillette, D. A., 1996. Calibration of GOES-VISSR, visible-band satellite data and its application to the analysis of a dust storm at Owens Lake, California ,*Geomorphology* 17,pp.229-250.

Mahowald, N., Baker, A., Bergametti, G., Brooks, N., Duce, R., Jickells, T., Kubilay, N., Prospero, J. and Tegen, I., 2005. Atmospheric global dust cycle and iron inputs to the ocean, *Global Biogeochem. Cycles*, Vol.19, No.4, GB4025, doi: 10.1029/2004GB002402.

Mahowald, N., Ballentine, J. A., Feddema, J. and Ramankutty, N., 2007. Global trends in visibility: implications for dust sources, *Atmos. Chem. Physics*, 7, 3309-3339.

Mattis, I., Muëller, A. A. D., Wandinger, U. and Althausen, D., 2002. Dual wavelength Raman lidar observations of the extinction-to-backscatter ratio of Saharan dust, *Geophys. Res. Lett.*, 29(9), 1306, doi: 10.1029/ 2002GL014721.

Meloni, D., di Sarra, A., Pace, G., and Monteleone, F., 2006. Aerosol optical properties at Lampedusa (Central Mediterranean) –2. Determination of single scattering albedo at two wavelengths for different aerosol types, *Atmos. Chem. Phys.* 6, 715-727.

Meloni, D., di Sarra, A., Monteleone, F., Pace, G., Piacentino, S. and Sferlazzo, D. M., 2008. Seasonal transport patterns of intense Saharan dust events at the Mediterranean island of Lampedusa, *Atmos. Res.* 88, 134-148.

Moorthy, K. K. et al. 1999. Aerosol climatology over India: 1. ISRO GBR MWR network and database, ISRO GBR SR-03-99, Indian Space Res. Organ., Bangalore.

Moorthy, K. K., Babu, S. S., Sunilkumar, S. V., Gupta, P. K. and Gera, B. S., 2004. Altitude profiles of aerosol BC, derived from aircraft measurements over an inland urban location in India, *Geophys. Res. Lett.*, 31, L22103, doi:10.1029/2004GL021336.

Moorthy, K. K., Babu, S. S., and Satheesh, S. K., 2005. Aerosol characteristics and Radiative Impacts over the Arabian Sea during the Intermonsoon Season: Results from the ARMEX field campaign, *J. Atmos. Sci.*, 62, 192-206.

Moorthy, K.K., Babu, S. S., Satheesh, S. K., Srinivasan, J. and Dutt, C. B. S., 2007. Dust absorption over an inland the “Great Indian Dessert” inferred using group-based and satellite remote sensing, *Journal of Geophysical Research-Atmospheres*, 112, D9, D09206.

Morys, M., Mims, F. M., Hagerup, S., Anderson, S. E., Baker, A., Kia, J., and Walkup, T., 2001. Design, calibration, and performance of MICROTOPS-II handled ozone monitor and sun photometer, *J. Geoph. Res.* 106, 14573-14582.

Moulin, C., Lambert, C. E., Dayan, U. et al., 1998. Satellite climatology of African dust transport in Mediterranean atmosphere, *J. Geophys. Res.* 103, 13137-13144.

Muhs, D. R., Budahn, J. R., Prospero, J. M., and Carey, S. N., 2007. Geochemical evidence for African dust inputs to soils of western Atlantic islands: Barbados, the Bahamas and Florida, *Journal of Geophysical Research*, 112, doi: 10.1029/2005JF000445.

Nair, P. R., Parameswaran, K., Sunil Kumar, S. V. and Rajan, R., 2004. Continental influence on the spatial distribution of particulate loading over the Indian Ocean during winter season, *J. Atmos. Solar Terr. Phys.*, 66, 27-38.

Nair, V. S., Moorthy, K. K. and Babu, S. S., 2008. Size segregated aerosol mass concentration measurements over the Arabian Sea during ICARB, *J. Earth Science Systems*, 117, 315-323.

Nickovic, S., Kallos, G., Papadopoulos, A. and Kakaliagou, O., 2001. A model for prediction of desert dust cycle in the atmosphere, *J. Geophys. Res.* 106: 18113-18130.

Pace, G., di Sarra, A., Meloni, D., Piacentino, S. and Chamard, P., 2006. Aerosol optical properties at Lampedusa (Central Mediterranean). 1. Influence of transport and identification of different aerosol types, *Atm. Chem. Phys.* 6, 697-713.

Papadimas, C. D., Hatzianastassiou, N., Mihalopoulos, N., Querol, X. and Vardavas, I., 2008. Spatial and temporal variability of aerosol properties over Mediterranean basin based on 6 years (2000-2006) MODIS data, *J. Geophys. Res.* 113, D11205, doi:10.1029/2007JD 009189.

Piketh, S. J. and Walton, N. M., 2004. Characteristics of atmospheric transport of air pollution for Africa, *Air Pollution*, 4G, pp. 173-195.

Pérez, C., Nickovic, S., Baldasano, J. M., Sicard, M., Rocadenbosch, F. and Cachorro, V. E., 2006. A long Saharan dust event over the western Mediterranean: Lidar, Sun photometer observations and regional dust modeling, *Journal of Geophysical Research*, 111, D15214, doi:10.1029/2005JD006579.

Prasad, A. K., Singh, S., Chauhan, S. S., Srivastava, M. K., Singh, R. P. and Singh, R., 2007. Aerosol radiative forcing over the Indo-Gangetic plains during major dust storms, *Atmospheric Environment*, 41 (29), pp. 6289-6301. Prospero, J. M., Ginoux, P., Torres, O., Nicholson, S. E., Gill, T., 2002. Environmental characterization of global sources of atmospheric soil dust identified with Nimbus 7 Total Ozone Mapping Spectrometer (TOMS) absorbing aerosol product, *Rev. Geophys.* 40, doi:10.1029/2000RG000095.

Ramachandran, S., 2004. Spectral aerosol optical characteristics during the northeast monsoon over the Arabian Sea and the tropical Indian Ocean: 1. Aerosol optical depths and their variabilities, *J. Geophys. Res.*, 109, D19207, doi:10.1029/2003JD004476.

Ramanathan, V., et al. 2001. Indian Ocean Experiment: An integrated analysis of the climate and the great Indo-Asian haze, *J. Geophys. Res.*, 106(D22), 28,371 – 28,398.

Reagan, J. A., Thomason, L. W., Herman, B. M. and Palmer, J. M., 1986. Assessment of atmospheric limitations on the determination of the solar spectral constant from ground- based spectroradiometer measurements. *IEEE Trans. Geosci. Remote Sens.*, GE- 24, 258– 266.

Remer, L. A., Tanre, D., Kaufman, Y. J., Ichoku, C., Matoo, S., Levy, R., Chu, D. A., Holben, B. N., Dubovik, O., Ahmad, Z., Smirnov, A., Martins, J. V. and Li, R. R., 2002. Validation of MODIS aerosol retrieval over ocean. *Geophys. Res. Lett.* 29, doi:10.1029/2001GL013204.

Remer, L. A., et al. 2005. The MODIS aerosol algorithm, products, and validation. *J. Atmos. Sci.*, 62, 947-973.

Rodriguez, S., Querol, X., Alastuey, K. G. and Kakaliagou, O., 2001. Saharan dust contributions to PM₁₀ and TSP levels in Southern and Eastern Spain, *Atmos. Environ.* 35, 2433-2447.

Russell, P. B., and Coauthors, 1993. Pinatubo and pre-Pinatubo optical-depth spectra:

Mauna Loa measurements, comparisons, inferred particle size distributions, radiative effects, and their relationship to lidar data. *J. Geophys. Res.*, 98, 22 969–22 985.

Satheesh, S. K., Moorthy, K. K., Kaufman, Y. J. and Takemura, T., 2006a. Aerosol optical depth, physical properties and radiative forcing over the Arabian Sea, *Meteorol. Atmos. Phys.*, 91, 45-62.

Satheesh, S. K., Vinoj, V. and Moorthy, K. K., 2006b. Vertical distribution of aerosols over an urban continental site in India inferred using a micro pulse lidar, *Geophys. Res. Lett.*, 33, L20816, doi:10.1029/2006GL027729.

Schepanski, K., Tegen, I., Laurent, B., Heinold, B. and Macke, A., 2007. A new Saharan dust source activation frequency map derived from MSG-SEVIRI IR-channels, *Geophysical Research Letters*, 34, L18803, doi:10.1029/2007GL030168.

Schmid, B., and Wehrli, C., 1995. Comparison of sun photometer calibration by use of the Langley technique and standard lamp. *Appl. Opt.*, 34, 4500–4512.

Shinn, E. A., Smith, G. W., Prospero, J. M., Betzer, P., Hayes, M. L., Garrison, V., Barber, R. T., 2000. African dust and the demise of Caribbean coral reefs, *Geophysical Research Letters* 27 (19), 3029–3032.

Slingo, A., et al. 2006. Observations of the impact of a major Saharan dust storm on the atmospheric radiation balance, *Geophys. Res. Lett.*, 33, L24817, doi:10.1029/2006GL027869.

Smirnov, A., Holben, B. N., Eck, T. F., Dubovik, O. and Slutsker, I., 2000. Cloud screening and quality control algorithms for the AERONET data base, *Remote Sens. Env.* 73, 337-349.

Sokolik, I., 2002. The spectral radiative signature of wind-blown mineral dust: implications for remote sensing in the thermal IR region, *Geophys. Res. Lett.* 29, 2154, doi:10.1029/2002GL015910.

Tegen, I., 2003. Modeling the mineral dust aerosol cycle in the climate system, *Quat. Sci. Rev.*, 22(19), 1821 – 1834, doi:10.1016/S0277-3791 (03)00163-X.

Torres, O., Bhartia, P. K., Herman, J. R., Ahmad, Z. and Gleason, J., 1998. Derivation of aerosol properties from satellite measurements of backscattered ultraviolet radiation: Theoretical basis, *J. Geophys. Res.*, 103, 17099–17110.

Torres, O., Tanskanen, A., Veiheiman, B., Ahn, C., Braak, R., Bhartia, P. K., Veefkind, P. and Levelt, P., 2007. Aerosols and surface UV products from Ozone Monitoring Instrument observations: an overview, *Journal of Geophysical Research*, 112, D24S47, doi: 10.1029/2007JD008809.

Tripathi, S. N., Dey, S., Tare, V., Satheesh, S. K., Lal, S. and Venkataramani, S. 2005. Enhanced layer of black carbon in a north India industrial city, *Geophys. Res. Lett.*, 32, L12802, doi:10.1029/2005GL022564. Vaughan, M., Young, S., Winker, D., Powell, K., Omar, A., Liu, Z. Hu, Y. and Hostetler, C., 2004. Fully automated analysis of space-based lidar data: an overview of the CALIPSO retrieval algorithms and data products, *Proc. SPIE*, 5575, pp. 16-30.

Washington, R., Todd, M., Middleton, N. J. and Goudie, A. S., 2003. Dust-storm source areas determined by the Total Ozone Monitoring Spectrometer and surface observations, *Annals of the Association of American Geographers*, 93, 2, 297-313.

Figure Captions

Figure 1. Spatial distribution of the wind speed and direction at 500 (a) and 700 hPa (b) at 12:00 UTC on 22 February 2008 over south Asia derived by MM5.

Figure 2. True visible Terra-MODIS image on 22nd and 23rd February 2008 above south Asia (a); False Color Composite (FCC) of Terra/Aqua – MODIS on 22nd February 2008 above AS. The dust plume is highlighted in both figures.

Figure 3. Temporal variation of the Terra (black) and Aqua (red) MODIS AOD₅₅₀ (a), FM (b) and Ångström exponent α in the spectral band 550-865 nm (c) values over south Asia. The values are averaged in the area 9-33 N_o, 49-78 E_o. The vertical bars show one standard deviation from the mean and are attributed to the spatial aerosol inhomogeneity.

Figure 4. Temporal variation of the Terra (a) and Aqua (b) MODIS-AOD₅₅₀ according to the latitude, before, during and after the dust event. The values are longitude-averaged in the area 49-78 E_o. The underlined areas correspond to individual dust-plume characteristics.

Figure 5. As in Fig. 4, but for the FM fraction.

Figure 6. Spatial distribution of the Terra-MODIS AOD₅₅₀ values on 22 February (a), and 23 February (b), as well as the respective FM fraction on 22 (c) and 23 (d) February, over south Asia.

Figure 7. Spatial distribution of the OMI-AI values from the Aura satellite on 22 (a) and 23 February over south Asia.

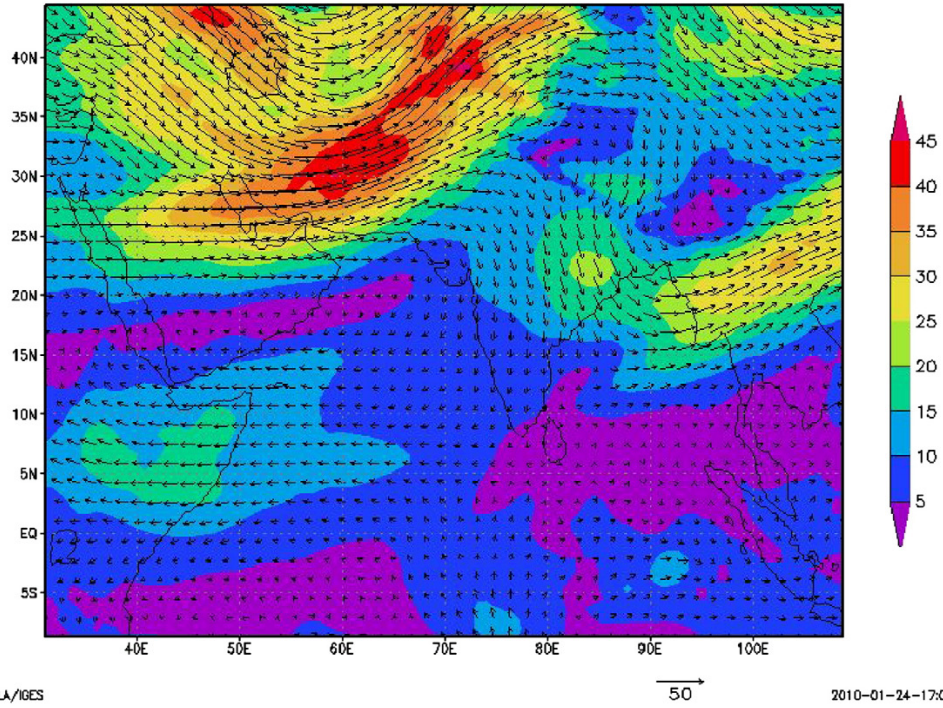
Figure 8. False Color Composite (FCC) images from the KALPANA-1 VHRR geostationary satellite at 06:00 (a), 09:00 (b), and 12:00 (c) UTC on 22 February, and at 05:00 UTC (d) on 23 February, over India.

Figure 9. Total attenuated backscatter profiles (km⁻¹ sr⁻¹) at 532 nm and the Vertical Feature Mask (VFM) image for daytime (08:30 UTC) (a) and nighttime (20:56 UTC) (b) conditions over south Asia obtained from CALIPSO observations. The VFM image divides the CALIPSO signal into seven categories. In the bottom of the figures the latitude (above) and the longitude (below) of the CALIPSO trajectory are also given. The whole CALIPSO trajectory is given in the upper panel of the figures, while the trajectory path is shown in blue.

Figure 10. Temporal variation of AOD₅₀₀ (a), Ångström exponent α in the spectral band 440-870 nm (b), coefficient a_2 from the polynomial fit $\ln AOD = a_2 \ln \lambda^2 + a_1 \ln \lambda + a_0$ (c), and FM fraction (d) from six AERONET stations in south Asia, before, during and after the dust event. The longitude of the stations corresponds to the colored scale (violet-to- red indicates west-to-east).

wswd 500hpa

22Feb08/12:00



wswd 700hpa

22Feb08/12:00

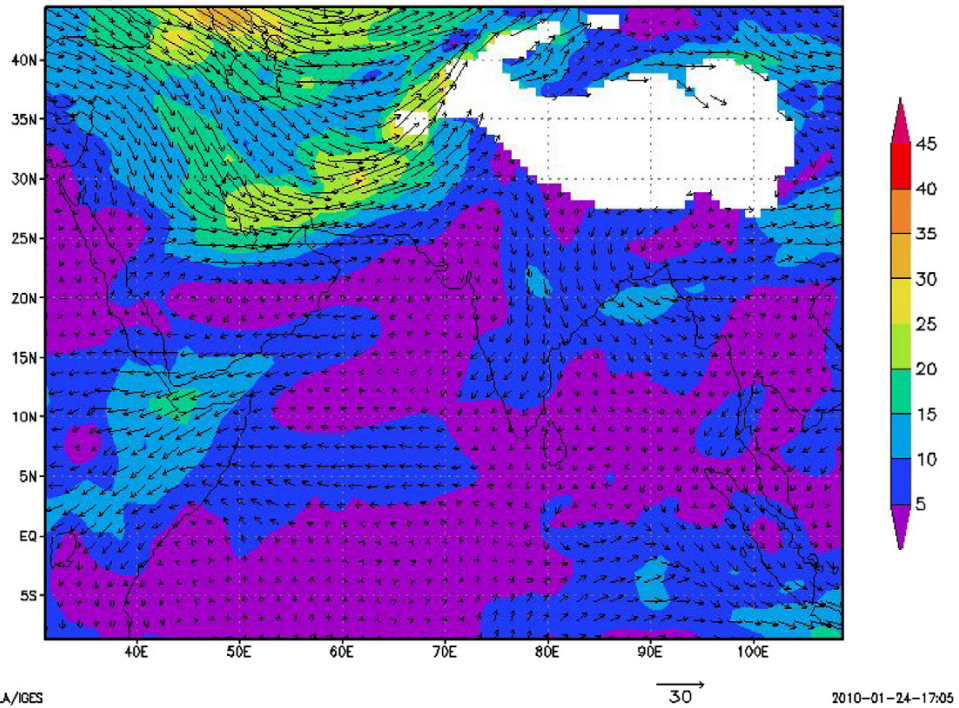
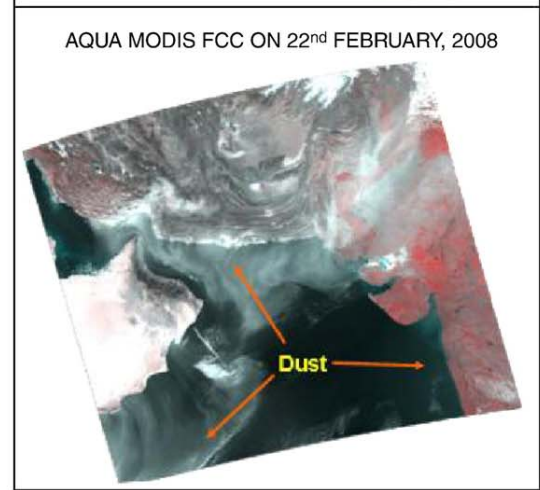
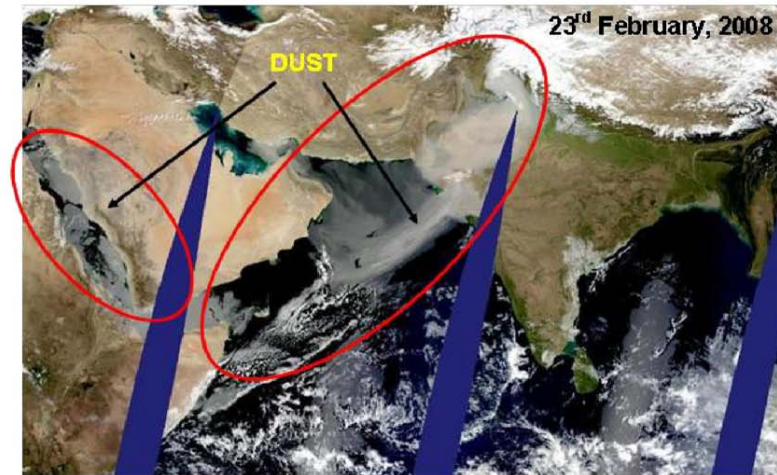
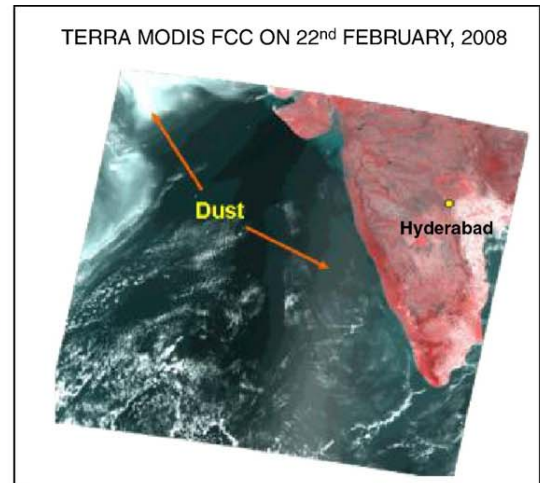
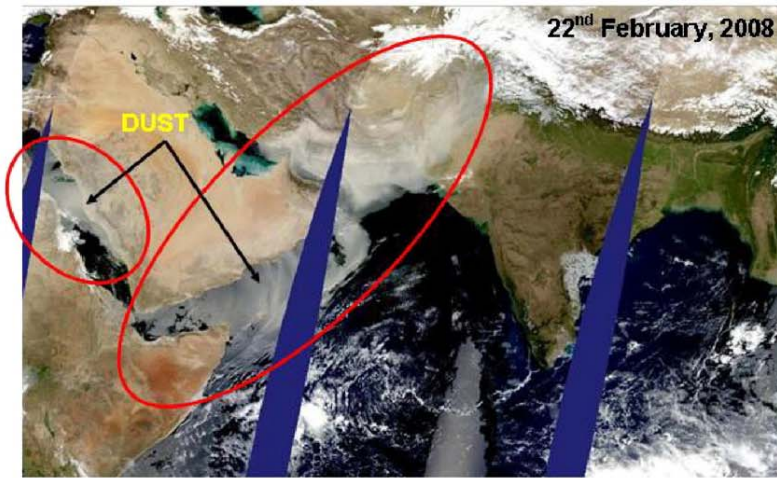


Figure 1.



(a)

(b)

Figure.2

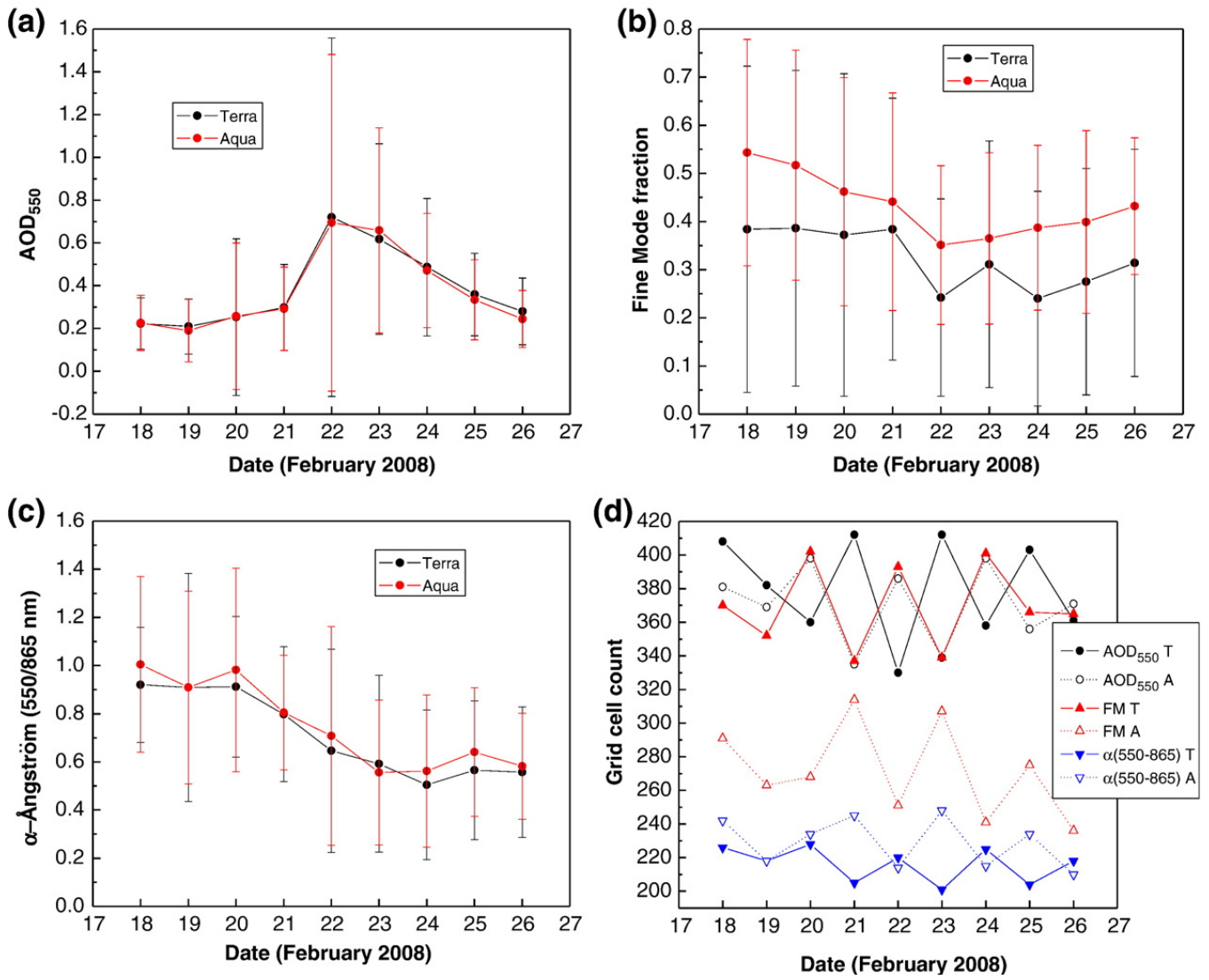


Figure 3

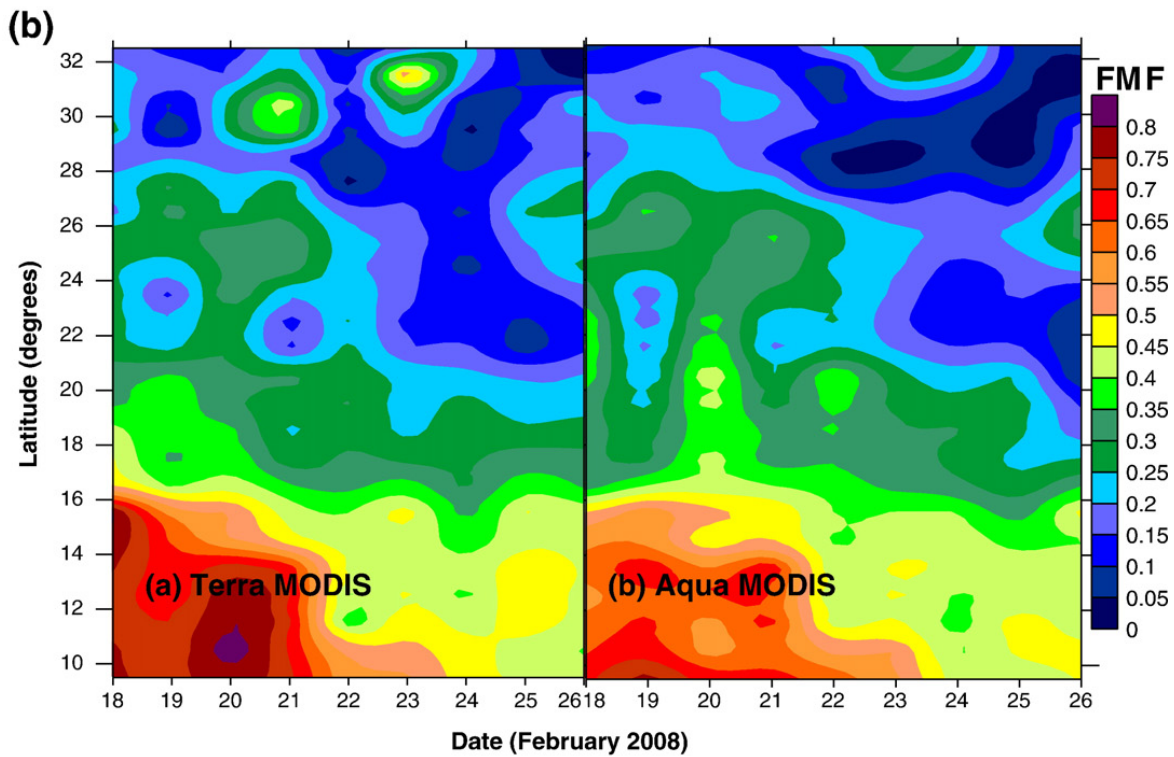
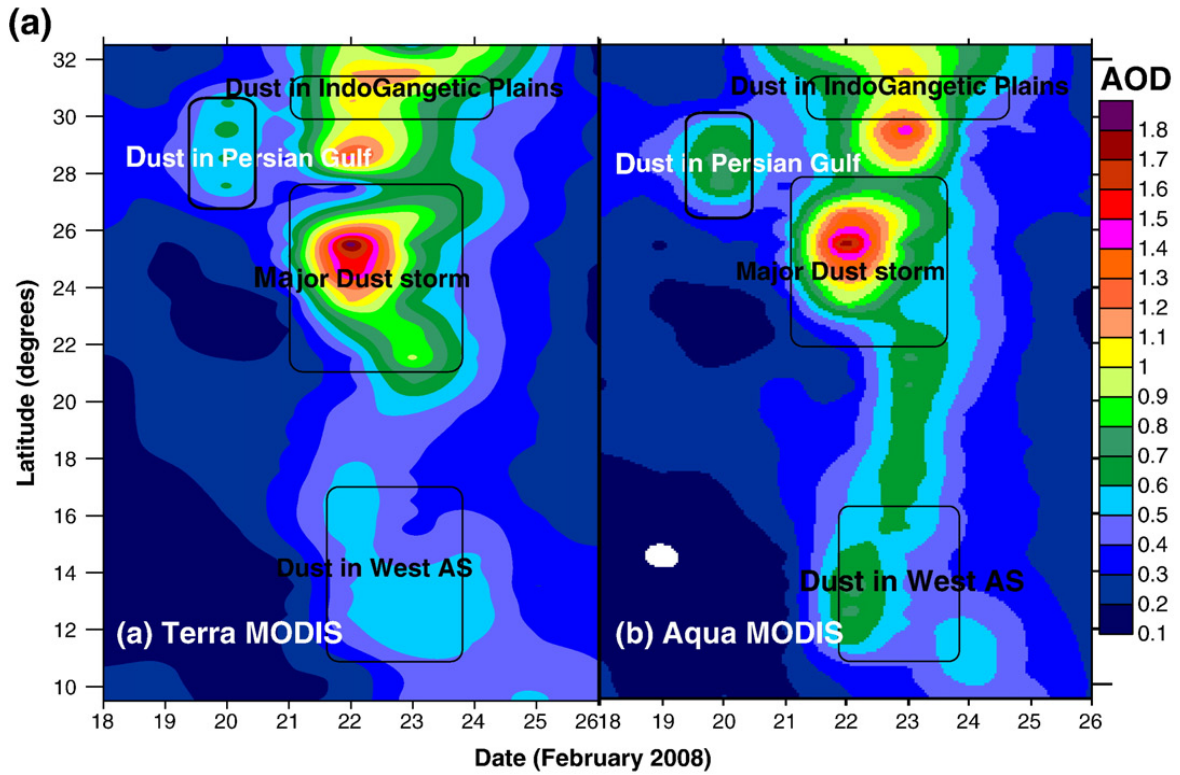


Figure 4

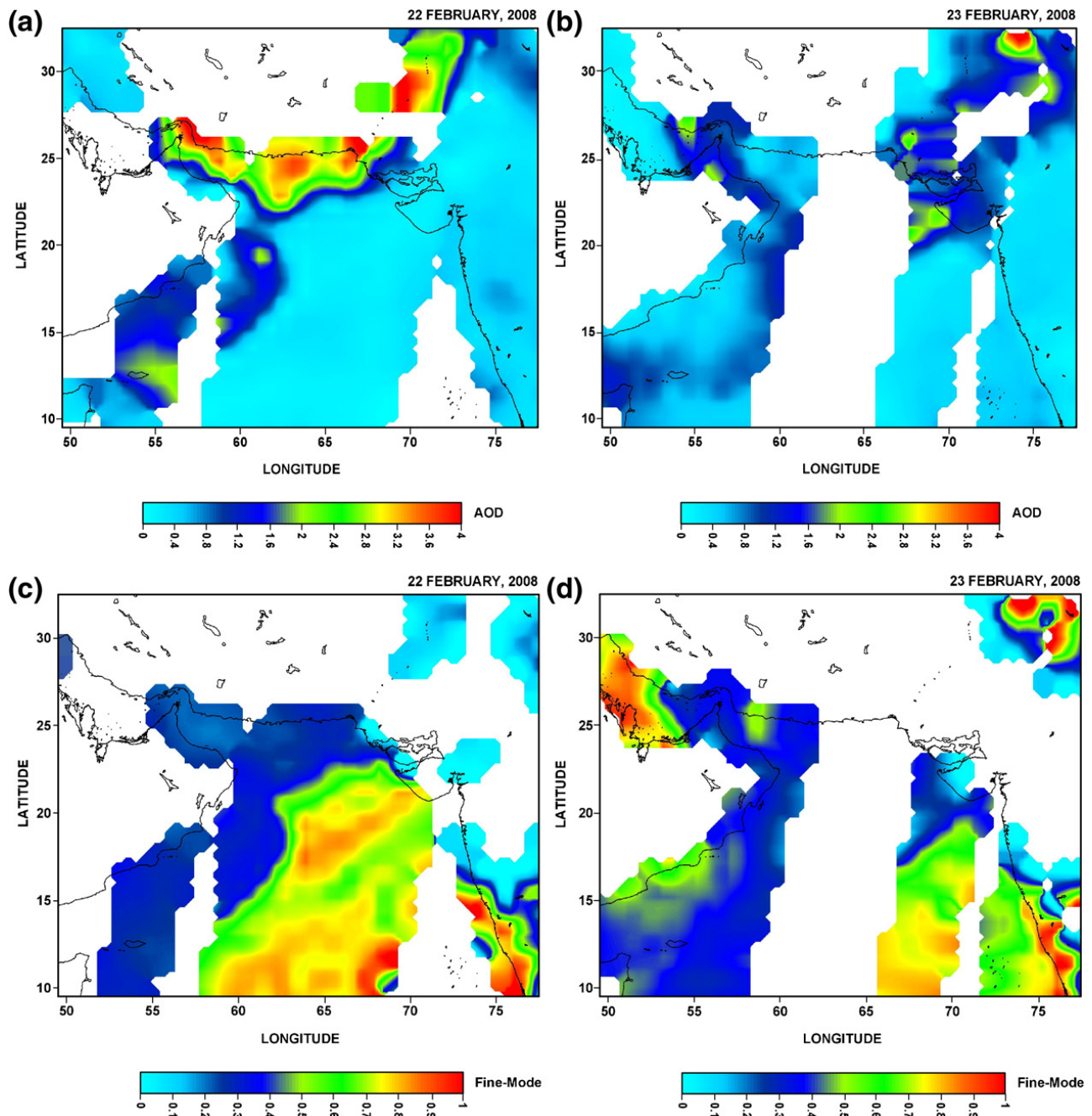


Figure 5

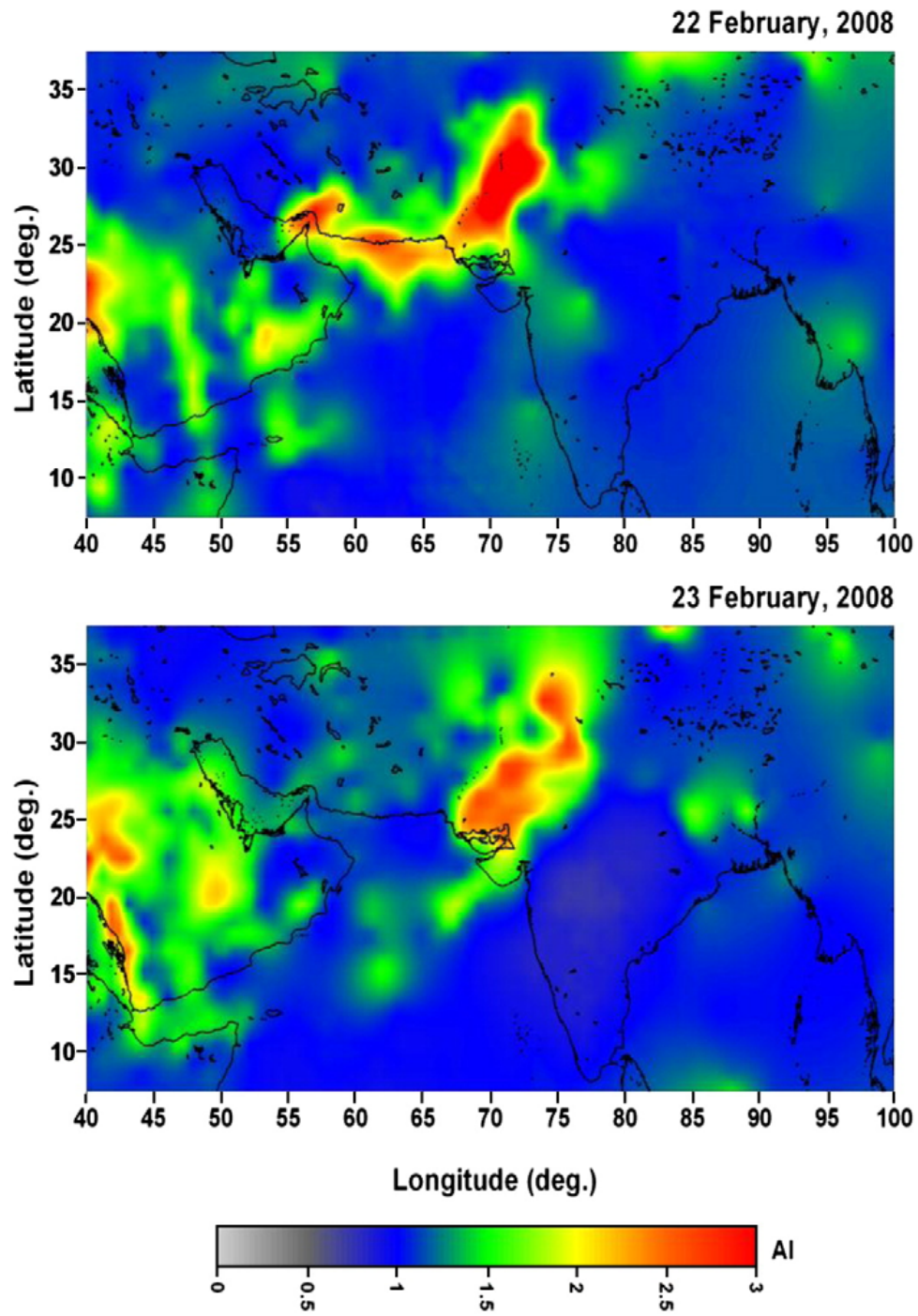


Figure 6

KALPANA - 1 VHRR FCC

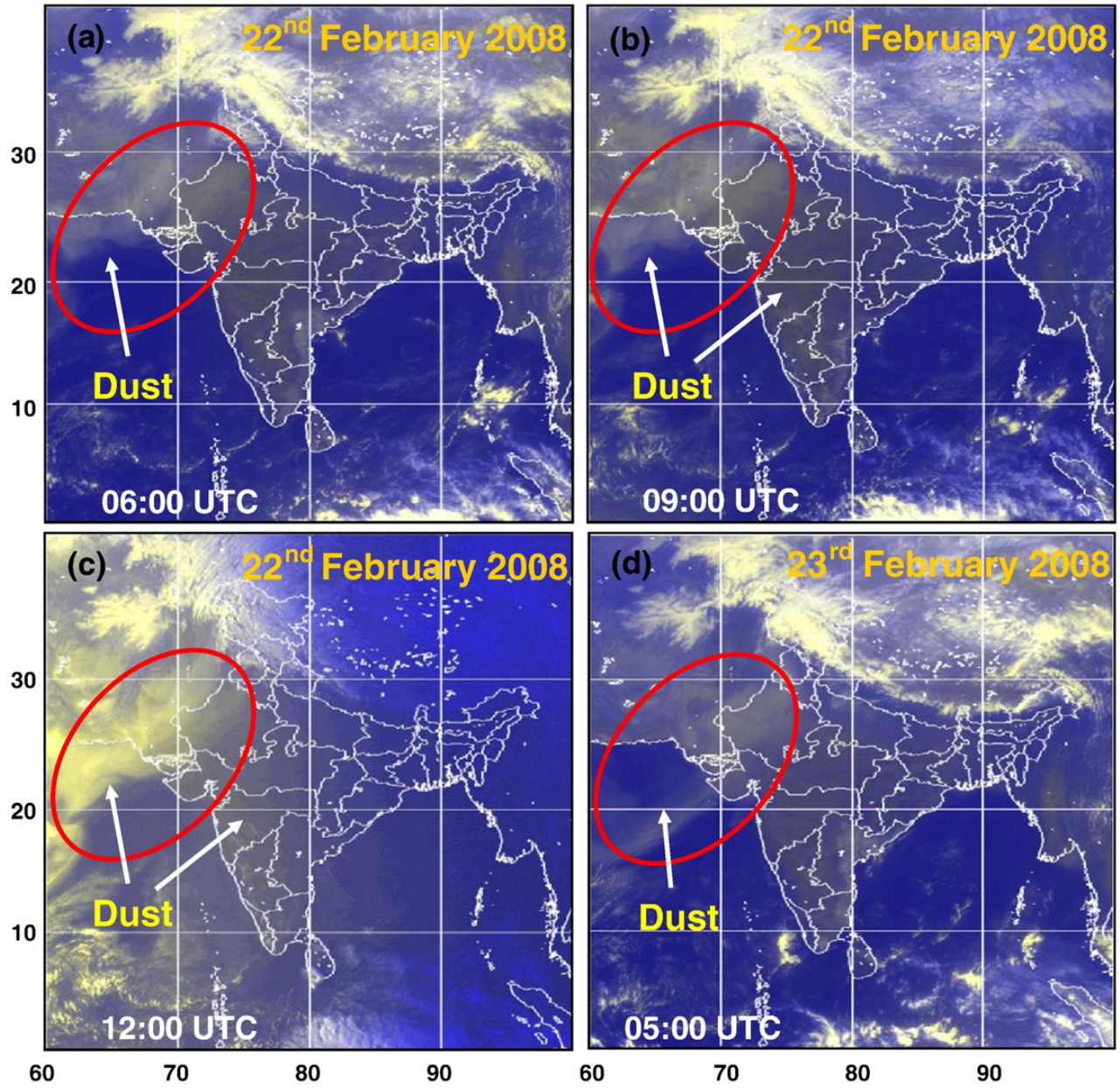
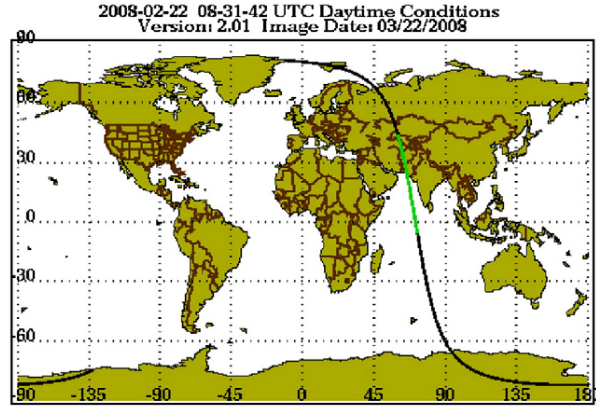


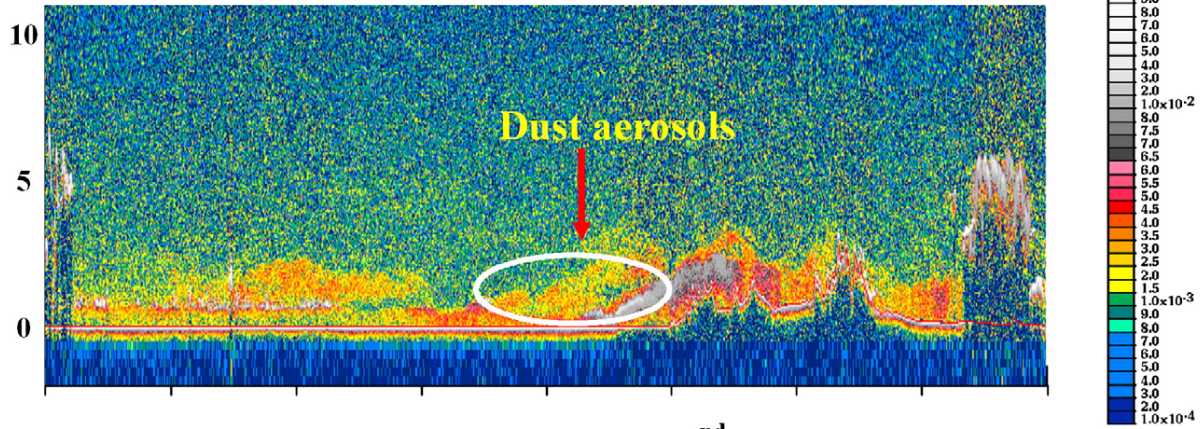
Figure 7

(a)

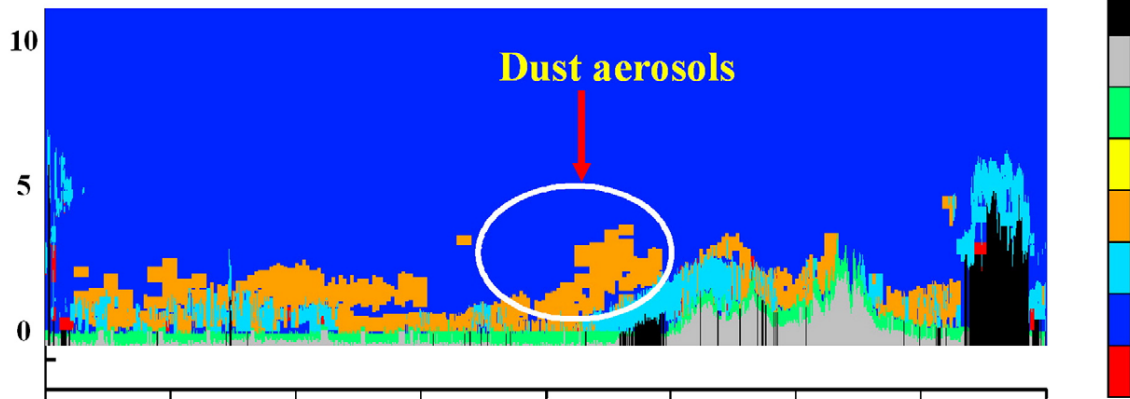
Daytime Conditions



532 nm Total Attenuated Backscatter ($\text{km}^{-1} \text{sr}^{-1}$) on 22nd February 2008



Vertical Feature Mask Image on 22nd February 2008

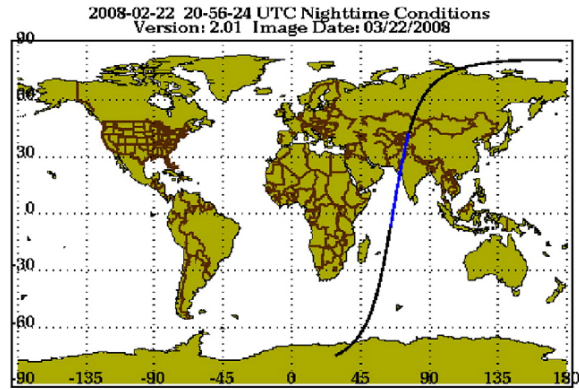


-5.05 1.02 7.13 13.24 19.35 25.45 31.54 37.60 43.65
72.00 70.71 69.41 68.08 66.70 65.25 63.69 61.97 60.03
Feature Type: 0 = Invalid (bad or missing data), 1 = Clear air, 2 = Cloud, 3 = Aerosol,
4 = Stratospheric feature, 5 = Surface, 6 = Subsurface, 7 = No signal (total attenuated)

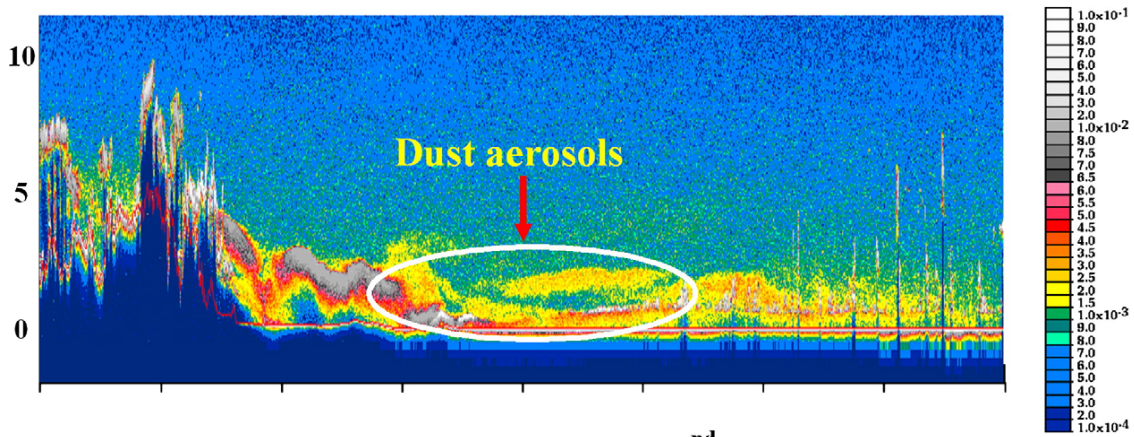
Figure 8a

(b)

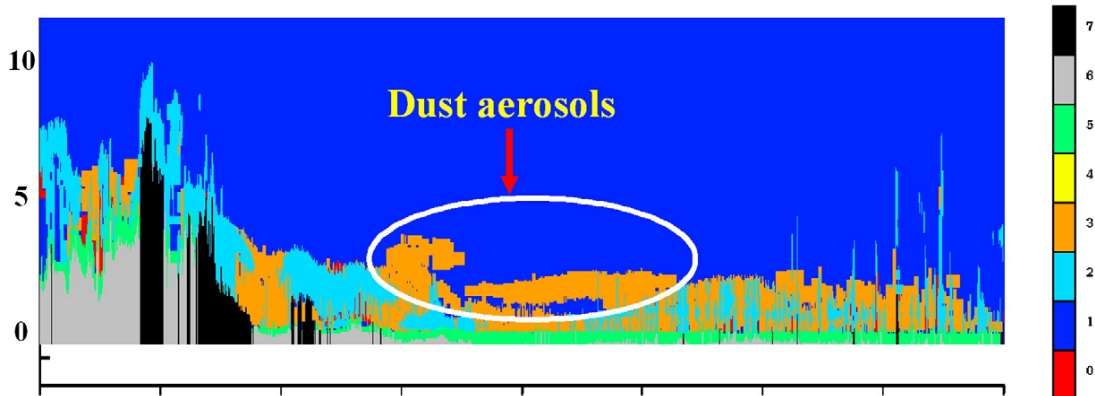
Nighttime Conditions



532 nm Total Attenuated Backscatter ($\text{km}^{-1} \text{sr}^{-1}$) on 22nd February 2008



Vertical Feature Mask Image on 22nd February 2008



42.50 36.45 30.38 24.29 18.19 12.08 5.97 -0.14 -6.26
76.05 74.16 72.47 70.94 69.50 68.14 66.82 65.51 64.21
Feature Type: 0 = Invalid (bad or missing data), 1 = Clear air, 2 = Cloud, 3 = Aerosol,
4 = Stratospheric feature, 5 = Surface, 6 = Subsurface, 7 = No signal (total attenuated)

Figure 8b

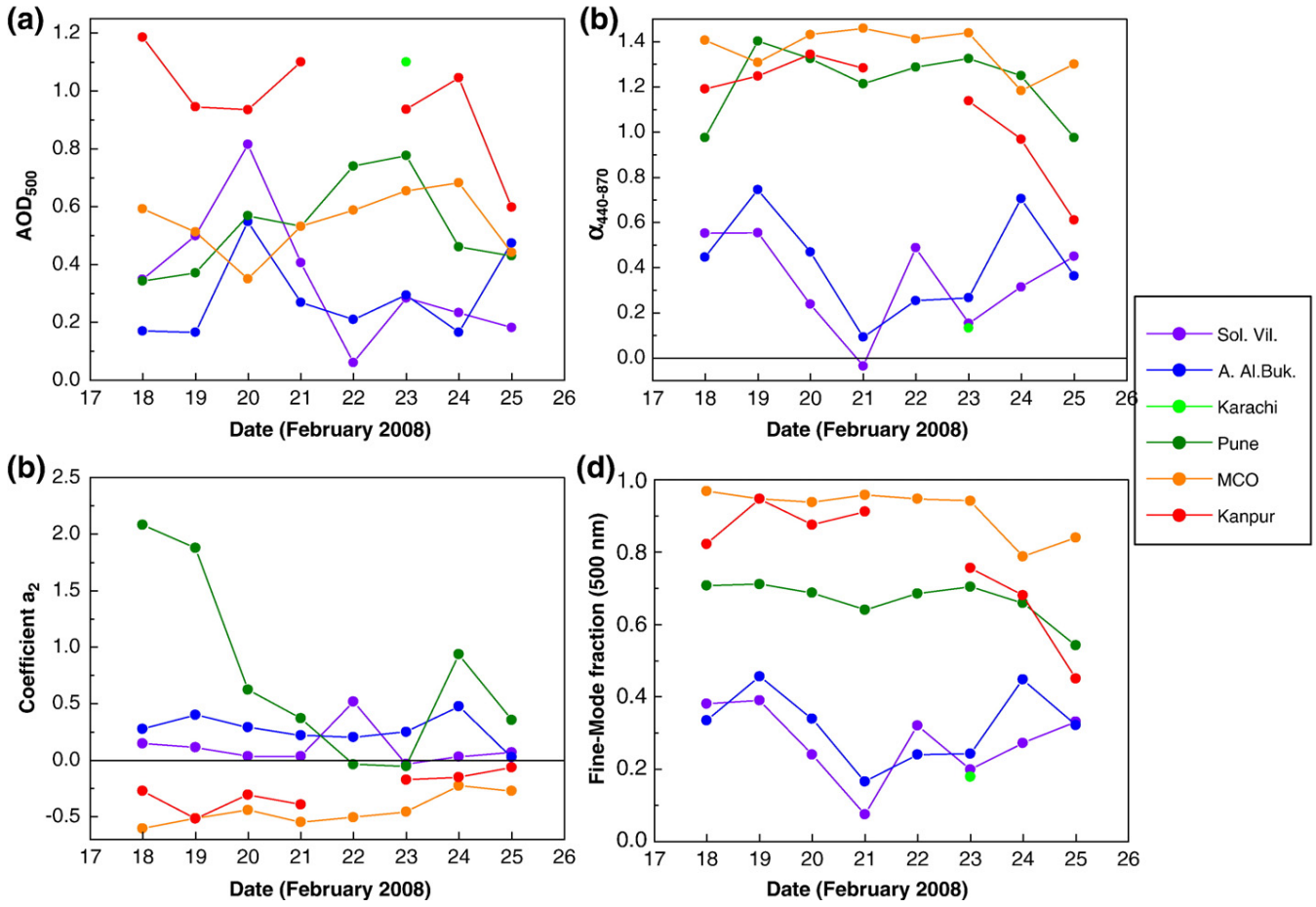


Figure 9

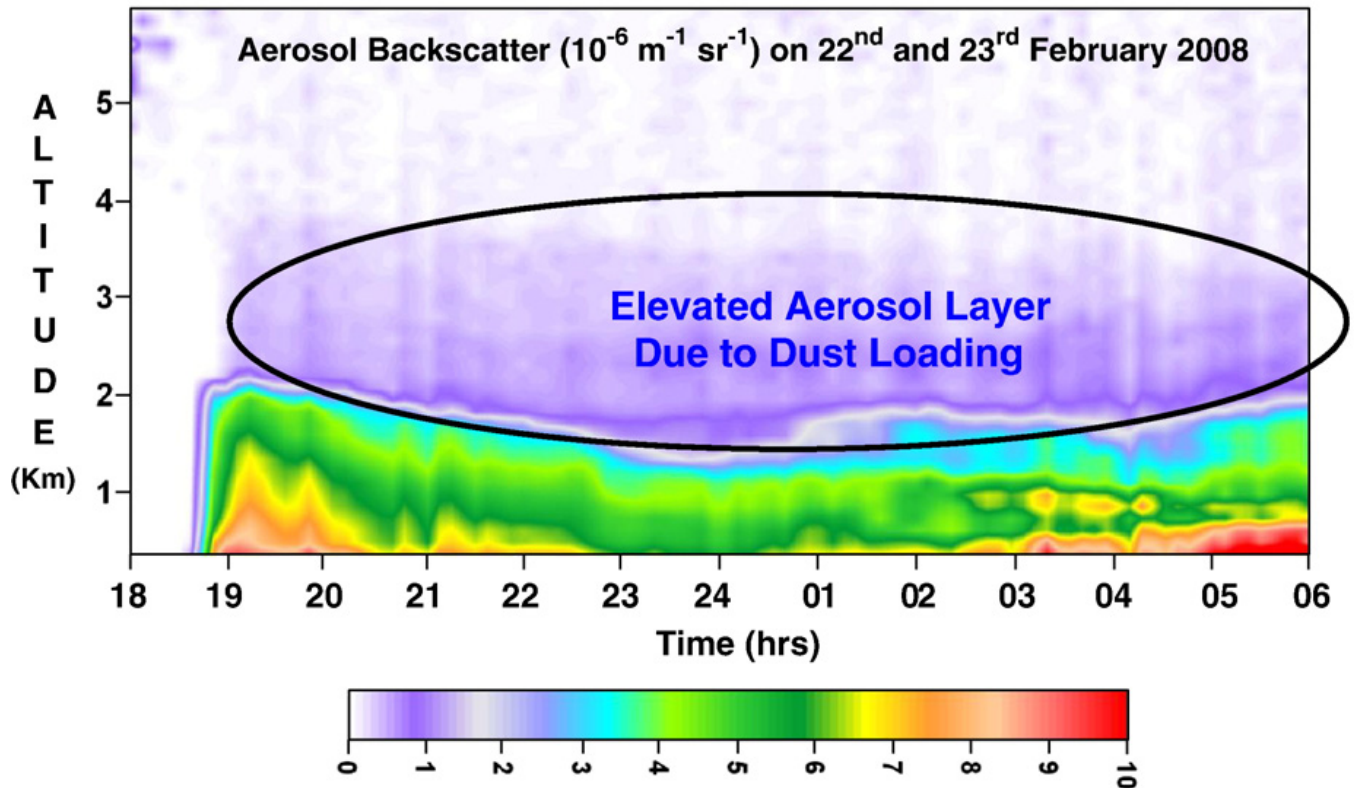


Figure 10

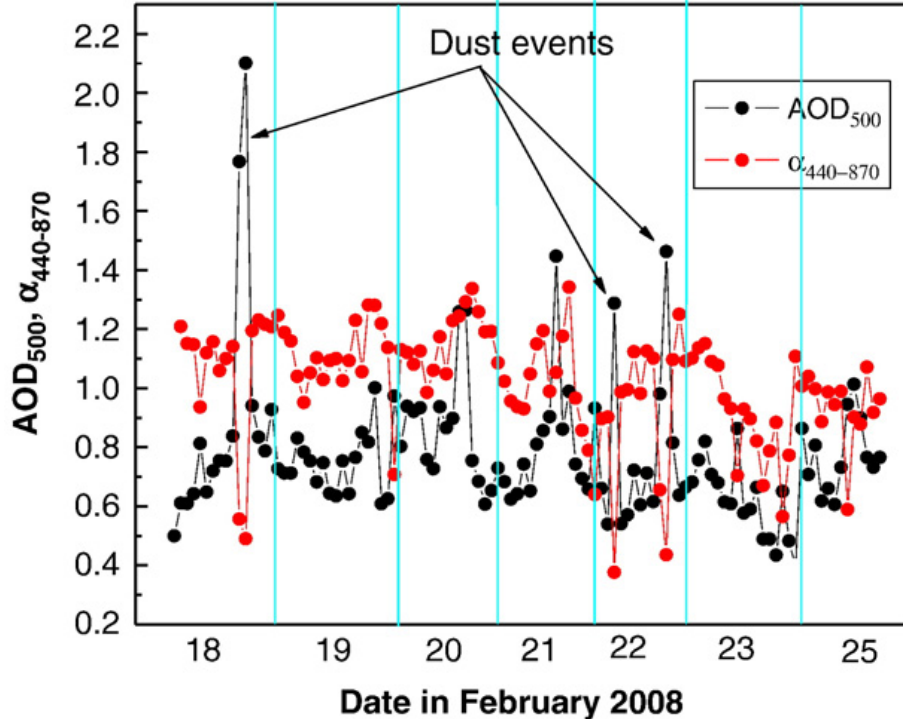


Figure 11

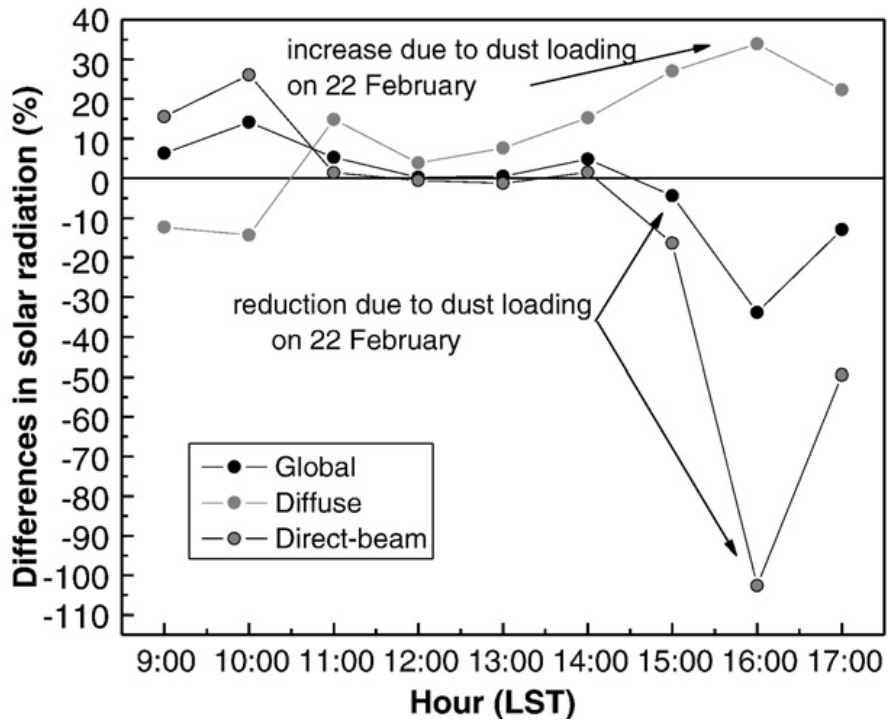


Figure 12

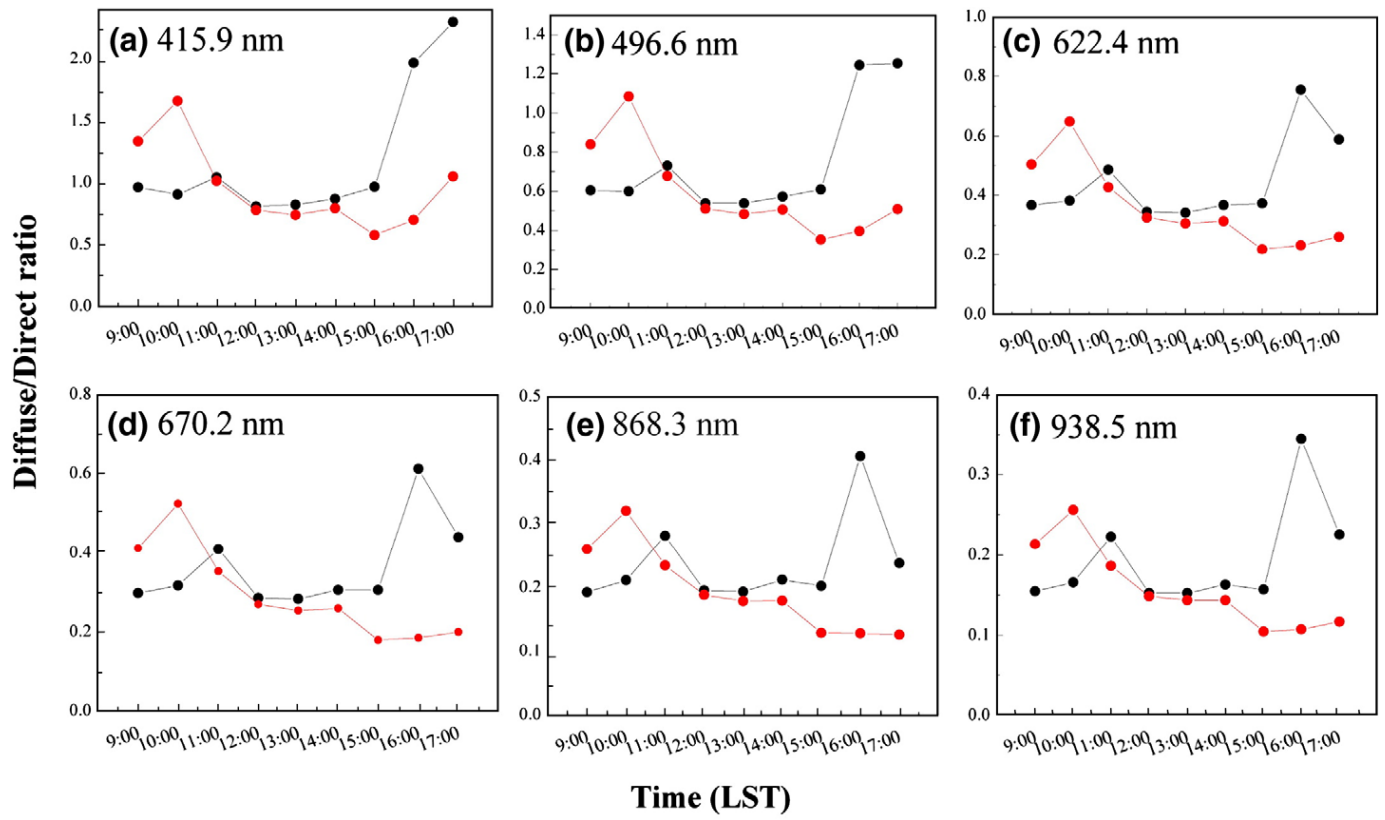


Figure 13